JACS
JOURNAL OF THE AMERICAN CHEMICAL SOCIETY
pubs.acs.org/JACS
Article

Assembly of Pyrenes through a Quadruple Photochemical Cascade: Blocking Groups Allow Diversion from the Double Mallory Path to Photocyclization at the Bay Region

Nikolas R. Dos Santos, João Vitor Schober, Croix J. Laconsay, Alexandria M. Palazzo, Leah Kuhn, Angel Chu, Benjamin Hanks, Kenneth Hanson, Judy Wu,* and Igor V. Alabugin*

Cite This: J. Am. Chem. Soc. 2025, 147, 1074−1091

ABSTRACT: We present a six-step cascade that converts 1,3-distyrylbenzenes (*bis*-stilbenes) into nonsymmetric pyrenes in 40−60% yields. This sequence merges photochemical steps, *E*,*Z*-alkene isomerization, a 6π photochemical electrocyclization (Mallory photocyclization); the new bay region cyclization, with two radical iodine-mediated aromatization steps; and an optional aryl migration. This work illustrates how the inherent challenges of engineering excited state reactivity can be addressed by logical design. An unusual aspect of this cascade is that the same photochemical process (the Mallory reaction) is first promoted and then blocked in different stages within a photochemical cascade. The use of blocking groups is the key feature that makes simple *bis*-stilbenes suitable substrates for directed double cyclization. While the first stilbene subunit undergoes a classic Mallory photocyclization to form a phenanthrene intermediate, the next ring-forming step is diverted from the conventional Mallory path into a photocyclization of the remaining alkene at the phenanthrene's bay region. Although earlier literature suggested that this reaction is unfavorable, we achieved this diversion via incorporation of blocking groups to prevent the Mallory photocyclization. The two photocyclizations are assisted by the relief of the excited state antiaromaticity. Reaction selectivity is controlled by substituent effects and the interplay between photochemical and radical reactivity. Furthermore, the introduction of donor substituents at the pendant styrene group can further extend this photochemical cascade through a radical 1,2-aryl migration. Rich photophysical and supramolecular properties of the newly substituted pyrenes illustrate the role of systematic variations in the structure of this classic chromophore for excited state engineering.

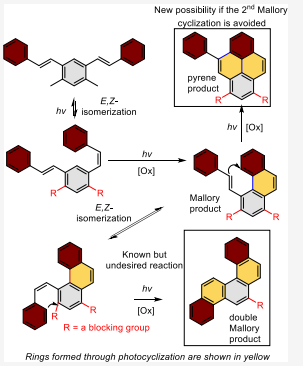

INTRODUCTION

Pyrene is the smallest stable peri-fused polyaromatic system and an important component of organic semiconductors with applications in OFETs (organic field-effect transistors),[1] organic thin-film transistors, and OLEDs (organic light-emitting diodes).[2−17] Pyrene's ability to form excimers in solution, long-lived excited states, and high fluorescence quantum yield have also made this chromophore useful as a blue-emitting fluorescent probe for biological analysis.[18−20] Despite this utility, synthetic approaches to make highly functionalized pyrenes are limited, and new selective approaches to complex substituted pyrenes are desired.

Synthetic approaches to pyrenes rely on two main strategies. The first one is to functionalize an existing pyrene core.[21−28] In this method, while mono functionalization of pyrenes is well explored, multiple selective functionalizations are challenging. The second, potentially more general, strategy relies on forming the pyrene core de novo via cyclizations of prefunctionalized starting materials.[3,4,29−38] For example, [2,2]-metacyclophanes can be nitrated and oxidized to substituted tetrahydropyrene (THPY) which can be further oxidized to pyrene in a subsequent step (Scheme 1a).[3,39] Photochemical activation of 2,2′-divinyl biphenyls can convert them into a THPY intermediate, which is then converted into pyrene after an additional oxidation step (Scheme 1b).[34,35] The pyrene core can also be assembled via a metal-catalyzed cyclization of *o*,*o*-diethynyl biphenyls (Scheme 1c)[40−43] or via radical *bis*-*peri*-annulation of 1,4-disubstituted naphthalenes (Scheme 1d).[37] However, even though these examples are conceptually interesting and practically useful, they readily apply only to symmetric pyrene derivatives.

We recently published an approach for the construction of nonsymmetric substituted pyrenes (Scheme 1e) via two sequential radical cyclizations.[44] This cascade takes advantage of aryl and vinyl radicals generated via two cooperative, consecutive pathways. Since these radicals are formed sequentially, the formation of the first cycle creates the necessary geometric environment for the formation of the

Received: October 15, 2024
Revised: December 12, 2024
Accepted: December 13, 2024
Published: December 27, 2024

https://doi.org/10.1021/jacs.4c14486
J. Am. Chem. Soc. 2025, 147, 1074−1091

Scheme 1. Examples of the De Novo Assembly of a Pyrene Core: (A) [2,2]-Metacyclophane Transannular Ring Closures Followed by Oxidation; (B) Biphenyl Photocyclization to Tetrahydropyrene Followed by Oxidation to Pyrene; (C) Radical Peri-Annulation of Naphthalene Cores; (D) Metal-Catalyzed Double Cyclization of *O,O*-Diethynyl Biphenyls; (E) Radical Peri Annulations of *Bis*-Alkynes; (F) Photochemical Cascade Suggested in This Work

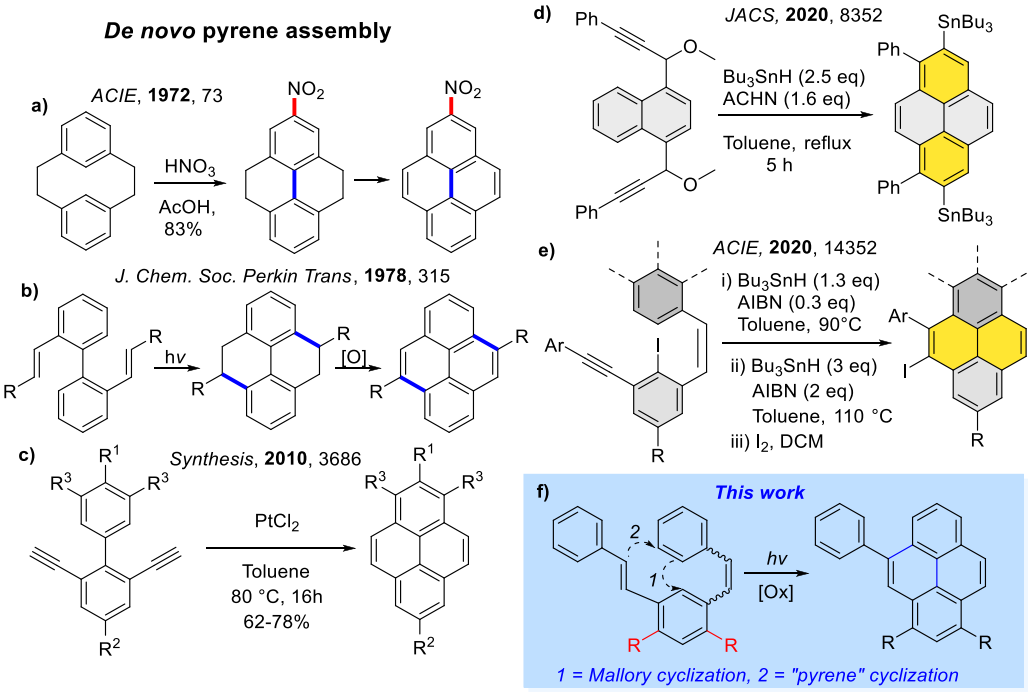

Scheme 2. (A) Possible Pathways of Photocyclization of *Bis*-Stilbenes Reported by Laarhoven et al.[45,48] and Morgan et al.[45] (B) Blocking Group Strategy for the Selective Synthesis of Pyrenes[a]

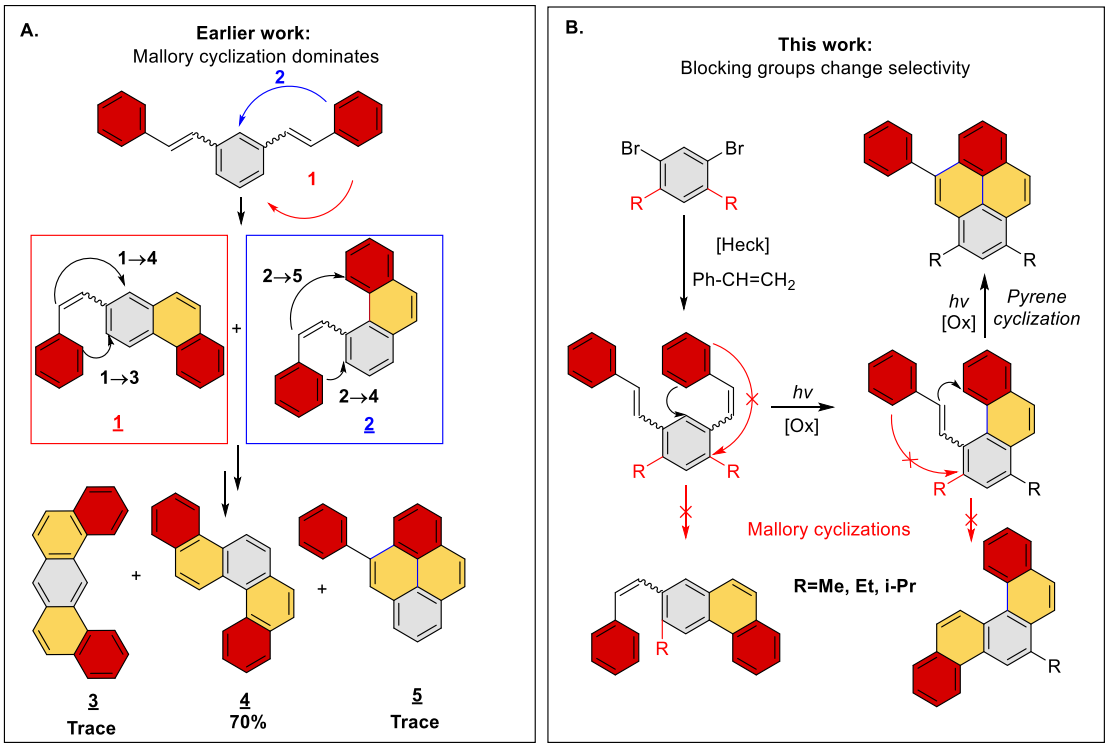

[a]Note the double role of blocking groups in the control of Mallory cyclization: directing regioselectivity in the 1st step and preventing this cyclization in the 2nd step.

second cycle. However, precursors to the enyne starting material require multistep synthesis; thus, being able to make pyrenes from easily assembled starting materials would be beneficial.

https://doi.org/10.1021/jacs.4c14486
J. Am. Chem. Soc. 2025, 147, 1074−1091

Scheme 3. Initial Results of *Bis*-Stilbene Photocyclizations Yielding Pyrene and Chrysene Products

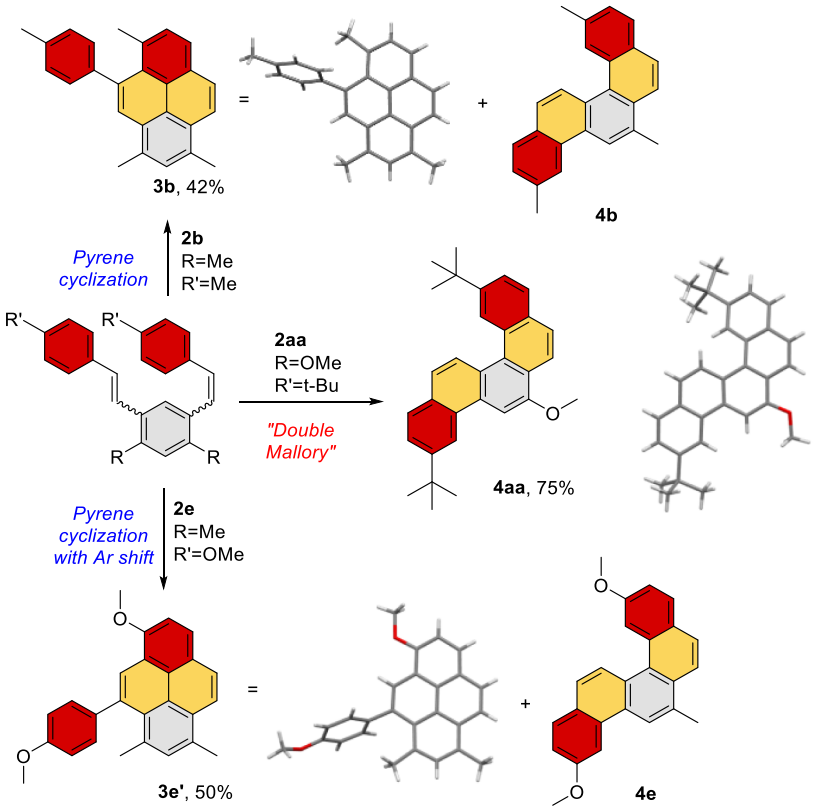

Considering that, we were intrigued by a potential assembly of the pyrene core from *meta-bis*-styrylbenzenes via a one-pot sequence of photochemical transformations (Scheme 1f). The *bis*-stilbene precursors are readily available in a single step from Heck coupling of 1,3-dihalosubstituted benzenes with styrenes. However, even though the cascade appears simple, it suffers from an intrinsic, internal contradiction. The first step of this cascade would include stilbene photocyclization (i.e., the Mallory reaction, vide infra), while the second step should avoid the Mallory reaction and, instead, undergo the unknown stilbene cyclization at the bay area of phenanthrene. So, on one hand, we needed the Mallory cyclization to proceed well (in the first step), but we also needed the Mallory cyclization to not proceed at all (in the second step).

As expected, the photochemistry of this simple system has been explored earlier. Laarhoven et al. and Morgan et al. were able to detect the formation of the target pyrene **5** after UV-irradiation of 1,3-distyrylbenzene (Scheme 2a).[45−47] However,[48] pyrene was formed only in "trace amount" while the other two products, including the main product, i.e., chrysene **4**, were produced via a sequence of two Mallory cyclizations.

Mallory cyclization is a classic photochemical electrocyclic transformation of a stilbene that yields a dihydrophenanthrene product. It became an important synthetic tool in 1964 when Mallory[49−52] discovered that the reaction could be promoted by the addition of iodine in the presence of O_2.[44,50] Its scope and efficiency were improved even further when Katz introduced the use of propylene oxide for quenching the HI byproduct.

Although literature precedent suggested that the Mallory reaction is the dominant path for the photochemistry of the parent 1,3-distyrylbenzene while the tantalizingly simple path to pyrenes is unlikely, we were not discouraged by these earlier reports.[53−55] If the formation of trace amounts of pyrenes is possible, then disfavoring the second Mallory cyclization might be sufficient to allow the slower cyclization to pyrene to become kinetically viable. In this work, we decided to explore if we can suppress the Mallory reaction and direct this transformation toward substituted pyrenes by using strategically positioned blocking groups R (Scheme 2b).

Our hopes for success in finding a suitable blocking group were also boosted by the known reversibility of the Mallory cyclization. Even if the R group does not prevent the cyclization, the dihydrophenanthrene intermediate could revert to stilbene, so the cascade can self-correct, as long as it does not undergo elimination, leading to aromatization.

In summary, the proposed photochemical sequence would start with a classic Mallory cyclization converting a stilbene subunit into a phenanthrene substituted at the bay region. The desired regioselectivity of this step is controlled by the presence of the first blocking group. In our plan, the second cyclization would avoid the Mallory pathway due to the presence of a second blocking group and proceed, instead, at the bay region with the formation of the target pyrene **5**.

Furthermore, this modular approach to substituted pyrenes takes advantage of easily available starting materials. The cyclization precursors can be prepared expediently via a double Heck cross-coupling of styrenes with commercially available 1,5-dihalo-2,4-dialkylbenzenes. The advantage of the photochemical approach is that the initial *E,Z*-stereochemistry of the stilbene precursors is inconsequential, as stilbene *E*- and *Z*-isomers interconvert under photoirradiation.[56−59]

RESULTS AND DISCUSSION

Initial Photochemical Studies. Under Katz conditions, Mallory cyclization occurs preferably at unsubstituted aromatic

https://doi.org/10.1021/jacs.4c14486
J. Am. Chem. Soc. 2025, 147, 1074−1091

carbons, avoiding positions substituted by the OMe or Br groups.[60,61] Thus, we chose *bis*-stilbene **2aa** with R = OMe for the initial tests (Scheme 3, middle). The photoreaction of this *bis*-stilbene (1 equiv, [1.5 mM]) in the presence of I_2 (3 equiv) and propylene oxide (100 equiv) in quartz glassware with 254 nm excitation provided product **4aa** in 75% yield. The structure of this compound was unambiguously confirmed by X-ray crystallography.

This result showed that OMe is not a suitable group for blocking the second Mallory cyclization. The successful use of OMe and Br as blocking groups in the literature was based on the competition between two Mallory cyclizations (one at the substituted and another at the unsubstituted position). Indeed, this tool for selectivity control works well here, as the first Mallory reaction proceeds at the unsubstituted carbon. In contrast, the competition for the second ring closure is between two different reactions, i.e., the Mallory cyclization at the OMe-substituted position and the pyrene cyclization at an unsubstituted position. Hence, this observation is consistent with the pyrene-forming cyclization being relatively slow: slower than the Mallory cyclization at both the unsubstituted and OMe-substituted carbons.

Not discouraged by this result, we tested the effect of more robust methyl blocking groups in *bis*-stilbene **2b** (Scheme 3, top). To our delight, pyrene **3b** was formed as the major product, which was isolated in 42% yield. Recrystallization from a hexane/DCM mixture provided single crystals that were used to unambiguously determine the pyrene structure of **3b** by X-ray analysis (Scheme 3). Double Mallory product **4b** via the elimination of a Me group was identified as a minor product. Fortunately, the formation of pyrene was preferred in a 5:2 **3b:4b** ratio.

An even more interesting result was observed for the photochemical transformation of a *bis*-stilbene reactant with a *p*-OMe-substituted terminal aryl group. In this case, formation of the final product **3e′** included a 1,2-shift of the anisole moiety along the pyrene's K-region. The cascade proceeded in 50% yield with even better (5:1) selectivity relative to the double Mallory path (**3e′:4e**) (Scheme 3, bottom). This intriguing result indicated the presence of interesting electronic factors that were absent from the previously studied molecules.

These initial experiments revealed a mechanistically rich photochemical landscape. To explore it further, we concentrated on two questions. First, since the methyl blocking group was imperfect, we decided to explore whether bulkier alkyl blocking groups would improve the selectivity. Second, we were interested in exploring whether the bulkier blocking groups would also prevent the aryl migration in the reaction of *p*-OMe substituted *bis*-stilbene **2e**.

Optimizing Experimental Conditions. After determining that the new cyclization cascade was feasible, we optimized the reaction conditions. We varied the irradiation wavelengths from 250 to 360 nm and found that the best yield/time ratio was achieved with 310 nm irradiation (Table S1, Entry 3). When the stilbene solution was diluted to 0.9 mM (Table S1, Entry 9), the time of the reaction was improved with concurrent small improvements in the yield. Increasing the oxidant equivalents, however, had a significant effect on yield or reaction time (Table S1, Entries 8−10). Finally, solvent screening revealed that hexanes provided the highest yield and the cleanest reaction, minimizing side reactions (Table S1, Entries 12).

1,5-Dibromo-2,4-dialkyl benzenes were synthesized in moderate yields through direct bromination of *meta*-dialkylbenzenes with Br_2 in the presence of catalytic amounts of I_2 in DCM (Scheme S1). These compounds were used as cores for the synthesis of the *bis*-stilbenes. Due to the lack of established double Heck reaction procedures in the literature for similar precursors, optimization was necessary. The reaction conditions (Et_3N (2.2 equiv), PPh_3 (0.2 equiv), $Pd(OAc)_2$ (10 mol %), and the corresponding styrene (4 equiv) in MeCN) were selected based on established literature protocols for the Heck reaction. These conditions afforded the desired stilbene **2b** in a 35% yield (Table S2, Entry 1).[62] The yield improved to 38% when reaction temperature increased from 80 to 100 °C (Table S2, Entry 3). Lowering the concentration of the starting material from 1.5 to 0.9 mM increased the overall yield to 50% and reduced the reaction time to 3 h (Table S2, Entry 6).

The presence of bulkier R groups in the dibromo cores significantly impacted the yields of double Heck couplings, requiring further reevaluation of solvents, bases, and catalysts. Changing the solvent from MeCN to DMF allowed the formation of a fully homogeneous solution and improved the yields. This optimization was done by using the most available core with R = Me. The final reaction conditions (Et_3N (4.0 equiv), PPh_3 (0.4 equiv), $Pd(OAc)_2$ (20 mol %), and corresponding styrene (4 equiv) in DMF at 135 °C) provided the *bis*-stilbene **2b** in 60% yield (Table S2, Entry 7). Further increasing the temperature from 135 to 153 °C did not significantly impact reaction yields (Table S2, Entry 8). Other modifications, such as the addition of $AgSO_3CF_3$ (Table S2, Entry 13) and change of base or catalyst did not improve the yield (Table S2, Entries 9−15).

Although lower yields were observed for the aryl bromides with bulky substituents, the required *bis*-stilbenes were prepared expediently and in sufficient quantities for further photocyclizations except for R′ = *t*-Bu (Scheme 4). For all products, the yields shown correspond to a mixture of *E*/*Z* isomers. Next, we explored how different functional groups in stilbene would affect the reaction.

Effect of Substituent in the Stilbene Unit. *Substitution at the Terminal Aryl Group.* At first, we explored the effects of

Scheme 4. Scope of *Bis*-Stilbenes Obtained Through the Double Heck Reaction of Dibromides 1a−d With Styrenes

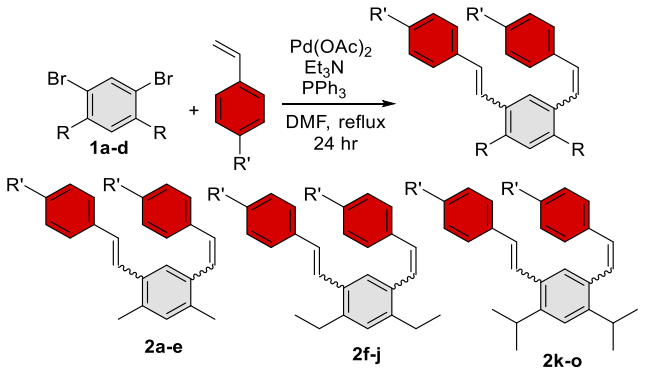

R'= H, 62%, **2a**
Me, 67%, **2b**
t-Bu, 45%, **2c**
Cl, 47%, **2d**
OMe, 72%, **2e**

R'= H, 35%, **2f**
Me, 31%, **2g**
Cl, 36%, **2i**
OMe, 39%, **2j**

R'= H, 23%, **2k**
Me, 20%, **2l**
Cl, 18%, **2n**
OMe, 30%, **2o**

https://doi.org/10.1021/jacs.4c14486
J. Am. Chem. Soc. 2025, 147, 1074−1091

substituent R′ in the terminal aryl group. The R′ groups varied from alkyl groups to electron withdrawing Cl and electron-donating OMe substituents. For R′ = H, good yields were observed with a 5:2 ratio of **3a:4a** (Scheme 5). After changing

Scheme 5. Scope of Pyrenes Synthesized by Changing R′ Groups[a]

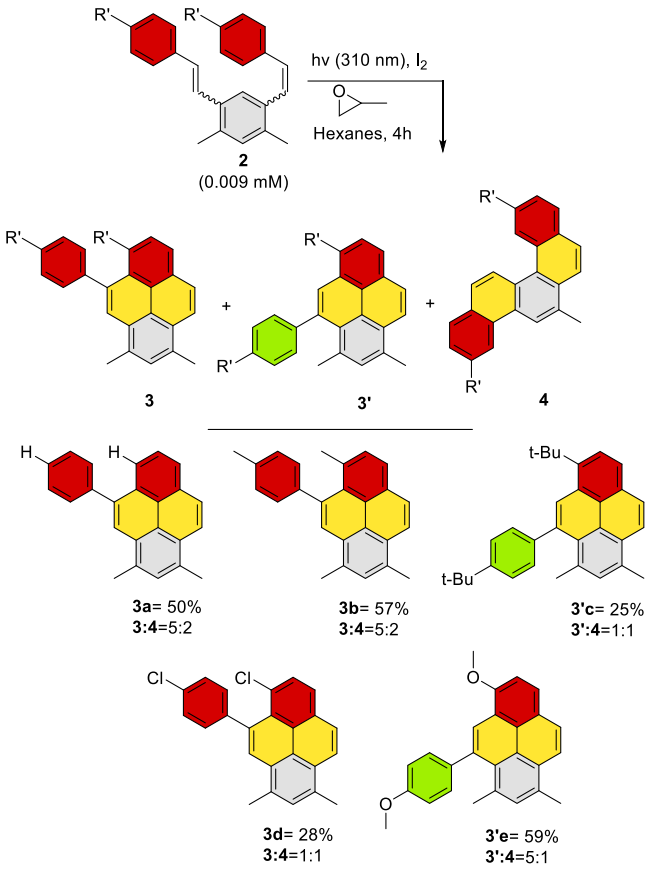

[a]Newly formed rings are shown in yellow, migrated aryl rings are shown in green.

R′ from H to a more donating Me group, yields increased from 50% to 57%, albeit without a noticeable change in the **3b:4b** ratio. Interestingly, while a larger alkyl substituent, R′ = *t*-Bu, had a negative effect on both yield and ratios, it also promoted the 1,2-Ar shift seen earlier with R = OMe, perhaps due to large steric assistance in the second cyclization step. As discussed earlier, substrates with R′ = OMe underwent [1,2]-migration of the pendant aryl ring after the desired double ring closure. This process was relatively efficient (59% yield) and selective, giving a higher ratio of pyrene to the double Mallory product (**3′:4** = 5:1). Photocyclization with the electron-withdrawing Cl group at the R′ position proceeded in lower yields, suggesting that the electronic effect of the halogen is unfavorable for this cascade.

Effect of the Blocking Group Size. A logical way to increase selectivity and prevent the Mallory reaction at the second cyclization stage would be to use bulkier blocking groups. To test this, we systematically varied the blocking groups R for each of the R′ substituents. The hypothesis was that the larger blocking groups would hinder the phenyl group from approaching the carbon site for the second Mallory cyclization. By increasing the size of the blocking groups, from methyl to isopropyl, we anticipated that this carbon site would become progressively less sterically accessible, thereby shifting the reaction balance toward pyrene formation.

However, the observed behavior was far more complex. For R′ = H, pyrene yield slowly decreased as the blocking group R increased in size (Me > Et > *i*-Pr for **3a, 3f,** and **3k**) while the **3:4** (i.e., "pyrene": "Mallory") selectivity also decreases, albeit very slightly, i.e., from 5:2 to 2:1 (Scheme 6). On the other hand, for R′ = Me, the yield increases significantly from **3b** to **3g** (R = Me and Et) before slightly dropping again for the more hindered **3L** (R = *i*-Pr). Interestingly, despite the lower yield, a slightly better selectivity was found for the bulkier R (**3:4** = 5:1).

For R′ = *t*-Bu/Cl (Scheme 5), both the yield and the ratio of products **3** to **4** decreased. Furthermore, the pyrene cyclization of the *t*-Bu-substituted substrate was accompanied by the 1,2-Ar shift, likely due to the steric assistance imposed by this bulky substituent.

For substrates with R′ = Cl and OMe, while the yields dropped slightly for bulkier blocking groups, the ratios of products improved, slightly favoring the formation of the pyrene product.

A possible explanation for these results is the tug-of-war between two factors acting in opposite directions. Although the larger blocking groups R slow down the Mallory reaction at the unintended site, they also serve as better leaving groups in the radical C−R scission (vide infra, Scheme 14), i.e., the step that makes the Mallory photocyclization irreversible. The two effects nearly cancel each other out, leading to an insignificant change in selectivity despite using significantly bulkier blocking groups.

With R′ = OMe R = Et/*i*-Pr, additional signals were identified through ^{1}H NMR, which could be attributed to the small amounts of nonrearranged pyrenes **3**. Unfortunately, these minor products were difficult to isolate due to their chromatographic similarity to the major products.

In summary, good selectivity and acceptable yields were observed for R′ = −H, -Me and -OMe for all the studied R blocking groups. The yields were slightly lower for R′ = -Cl, -*t*-Bu due to competition of double Mallory cyclization with the pyrene-forming pathway. However, considering that the overall synthetic path is short and inexpensive, the new cascade is still an efficient route to these tetrasubstituted pyrenes. Although the overall yields range between 20 and 67%, these pyrenes display complex unsymmetrical substitution patterns absent from the literature.

The cyclization of substrates with R′ = OMe and *t*-Bu proceeded with the additional 1,2-aryl shift step, although likely for different reasons. The *p*-OMe substituent has the donor ability needed to stabilize a possible electron-deficient intermediate responsible for the 1,2-shift (vide infra). On the other hand, the *t*-Bu group is likely to clash with the adjacent pendant aryl group, destabilizing the "normal" pyrene product. For a more detailed analysis of the structural effects of substituents at the pyrene core, see the SI part.

Functionalization of New Pyrenes. Pyrene can be divided into two regions, historically referred to as the K- and non-K-regions.[63] The non-K-region of pyrene is activated toward electrophilic aromatic substitution at positions 1, 3, 6, and 8,[64] while functionalization of positions 2 and 7 is possible when using bulky electrophiles and/or the assistance of transition metals (Scheme 7).[18,65] The K-region of pyrene is accessible only when the non-K-region is blocked. Partial reduction of the

https://doi.org/10.1021/jacs.4c14486
J. Am. Chem. Soc. 2025, 147, 1074−1091

Scheme 6. Scope of Pyrenes Synthesized by Changing Blocking R and R′ Groups: (A) Yields are NMR Yields and NMR Ratios

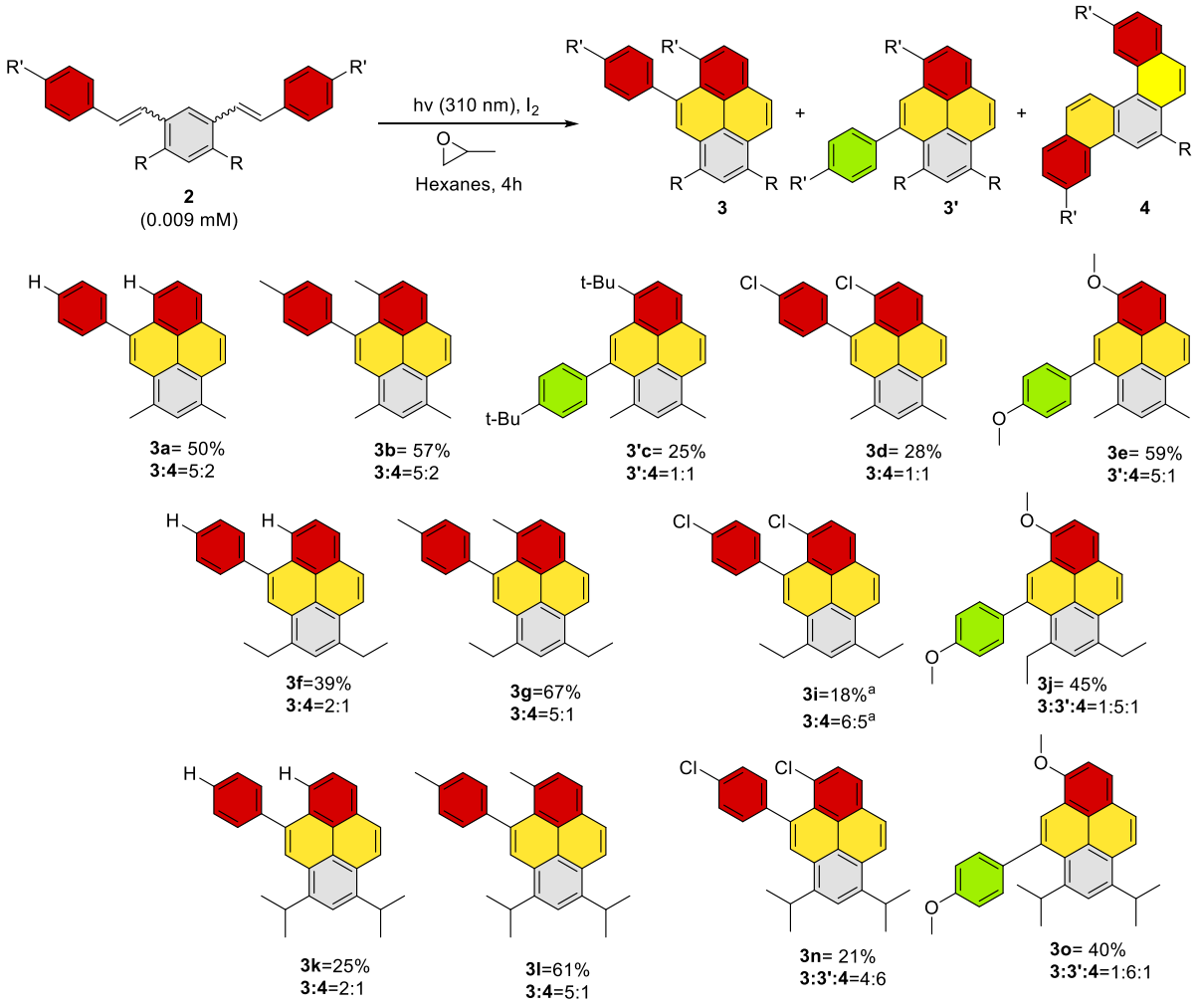

pyrene moiety, followed by its functionalization and rearomatization, offers additional synthetic opportunities, but, in general, synthesis of nonsymmetric poly substituted pyrenes remains difficult.[66]

Pyrenes **3a** and **3b** selectively reacted with electrophiles with the formation of 8-substituted products (Scheme 7). The high regioselectivity of substitution is consistent with the known preference for pyrene itself, and the fact that only one of the activated (1,3,6,8) positions in the pyrene starting material is not blocked by an alkyl substituent. Selective formation of aldehyde product **5c** is likely also assisted by steric factors. The selectivity was determined by X-ray crystallographic analysis for formylated product **5c** and by 2D NMR for the three other products. These reactions introduced convenient functional group handles that should facilitate the future incorporation of these nonsymmetric pyrenes into more complex molecules and materials.

Mechanism: Competition between the Two Cyclizations. This new multistep photochemical cascade provides a fertile ground for mechanistic analysis. The key stage is the competition between two cyclizations: the classic stilbene photocyclization (i.e., the Mallory reaction[60]) and the new "pyrene" cyclization.

To understand this competition, we modeled the photocyclization steps leading to pyrene **3b** vs chrysene **4b** (R = Me) in a 5:2 ratio with density functional theory calculations. Photocyclization from *bis*-stilbene to pyrene occurs via two sequential steps (Scheme 8). The first step is a classic stilbene Mallory reaction, which involves a conrotatory 6π-electrocyclic ring closure followed by oxidative aromatization.[67,68] In the second step, two competing 6π-electrocyclic reactions can occur. The electrocyclic ring closure at the bay region of phenanthrene **B** leads to intermediate **C**, which, upon oxidation, forms pyrene **3b**. Note that the pyrene cyclization can proceed through either an $\mathbf{B}_{trans}$ or $\mathbf{B}_{cis}$ stilbene isomer. A competing Mallory reaction of the *cis*-stilbene **B′** generates intermediate **D**, which forms chrysene **4b** upon oxidation. Structures $\mathbf{B}_{trans}$, $\mathbf{B}_{cis}$, and **B′** are nearly isoenergetic at the M06-2X(D3)/6-31+G(d) level, indicating that both **B** and **B′** are energetically accessible and present at the onset of the second photocyclization step.

Given the multistep nature and complexity of the cascade, direct experimental studies of the nature of reactive excited states (singlet vs triplet) for the pyrene-forming reaction are impractical. This makes computational methods particularly valuable for unraveling the role of excited states in the reaction mechanism. In the initial computational investigation, we explored both a singlet and a triplet state pathway for the competing cyclization reactions, $\mathbf{B}_{trans} \rightarrow \mathbf{C}$ vs $\mathbf{B}' \rightarrow \mathbf{D}$. Since $\mathbf{B}_{trans}$ is 0.1 kcal/mol lower in energy than $\mathbf{B}_{cis}$, we focused on the reaction profiles of $\mathbf{B}_{trans}$, as illustrated in Scheme 9. Computed free energy profiles for conrotatory electrocycliza-

https://doi.org/10.1021/jacs.4c14486
J. Am. Chem. Soc. 2025, 147, 1074−1091

Scheme 7. Selected Electrophilic Substitution Reactions of the New Pyrenes

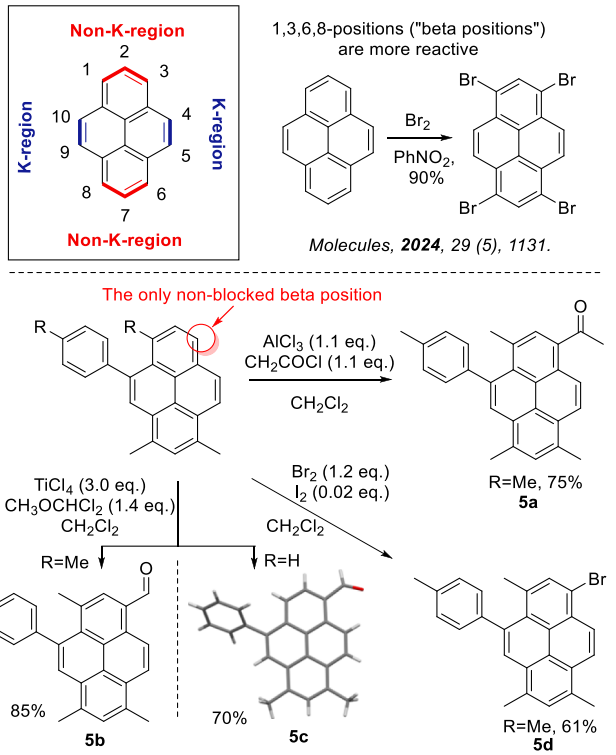

tion reactions in the S_0 and T_1 states are shown in the middle panels of Scheme 9. Single-point energies in the S_1 state were computed for the S_0 state minima geometries and for the S_0 state transition state structures. All of the reaction profiles were computed at the M06-2X(D3)/6-31+G(d) level.

Direct comparisons between the T_1 state reaction profiles for $\mathbf{B}_{trans} \rightarrow \mathbf{C}$ vs $\mathbf{B}' \rightarrow \mathbf{D}$ suggest that a triplet mechanism may be feasible for the pyrene-forming reaction but not for the Mallory reaction. $\mathbf{B}_{trans} \rightarrow \mathbf{C}$ proceeds through a small barrier (7.5 kcal/mol) and is exothermic, while $\mathbf{B}' \rightarrow \mathbf{D}$ faces a much higher barrier (24.0 kcal/mol) and is endothermic. These values predict that selectivity would be much higher than the modest experimental preferences if both reactions proceed exclusively through a triplet state, which is clearly not the case.

Hence, one or both reactions should proceed in the S_1 state. Calculations find that the Franck–Condon (FC) S_1 energies for $\mathbf{B}_{trans}$ (92.3 kcal/mol) vs $\mathbf{B}'$ (92.7 kcal/mol) are nearly identical. Notably, the energy drop between the Franck–Condon point and the S_1 energy at the S_0 transition state geometry is much steeper on the pyrene-forming cyclization path. The more favorable energy gradients on the path to the pyrene product (i.e., the nonstatistical effects[69−71]) may contribute to the 5:2 preference observed for **3b:4b**.

To get additional information about reaction energy profiles in the S_1 state, we performed relaxed potential energy profile scans along the forming C–C bond coordinate (see "*d*" in Scheme 9, top) at 0.1 Å intervals for structures $\mathbf{B}_{trans}$ and $\mathbf{B}'$ at TD-M06-2X(D3)/6-31+G(d) (represented by red dots in Scheme 9, bottom). Single-point energies in the S_0 state were computed at UM06-2X(D3)/6-31+G(d) for each S_1 geometry obtained from the relaxed potential energy profile scan (see black dots in Scheme 9, bottom). Relative energies of key reference points, i.e., the S_0 state minima and Franck–Condon points for $\mathbf{B}'$ and $\mathbf{B}$ are also included. A similar protocol was used by Oruganti, London, and Durbeej in their investigation of the cyclization reaction of a dithienylbenzene photoswitch.[72] While multireference computations with nonadiabatic molecular dynamics would provide a more accurate description of the nuances contributing to selectivity around the Franck–Condon region, the steeper downhill descent observed in the DFT and TD-DFT energy profile scans from the Franck–Condon point suggests a preference for the pyrene-forming reaction.

Specifically, the pyrene-forming pathway (Scheme 9a, bottom) shows a larger energy drop (24.4 kcal mol^{-1}) from the Franck–Condon point (92.3 kcal mol^{-1}) to the lowest energy point obtained on the S_1 state scan (67.9 kcal mol^{-1}). In comparison, the Mallory pathway (Scheme 9b, bottom) displays a smaller energy drop (12.9 kcal mol^{-1}) from the Franck–Condon point (92.7 kcal mol^{-1}) to the lowest point obtained on the S_1 state scan (79.8 kcal mol^{-1}). Qualitative differences in the energy profiles of the pyrene-forming and chrysene-forming reactions may contribute to the observed 5:2 product ratio for **3b:4b**. Furthermore, we note that the S_1

Scheme 8. Stages and Key Intermediates for the Sequential Photocyclization Reactions of *bis*-Stilbene Leading to Pyrene (3b) vs Chrysene (4b) Products

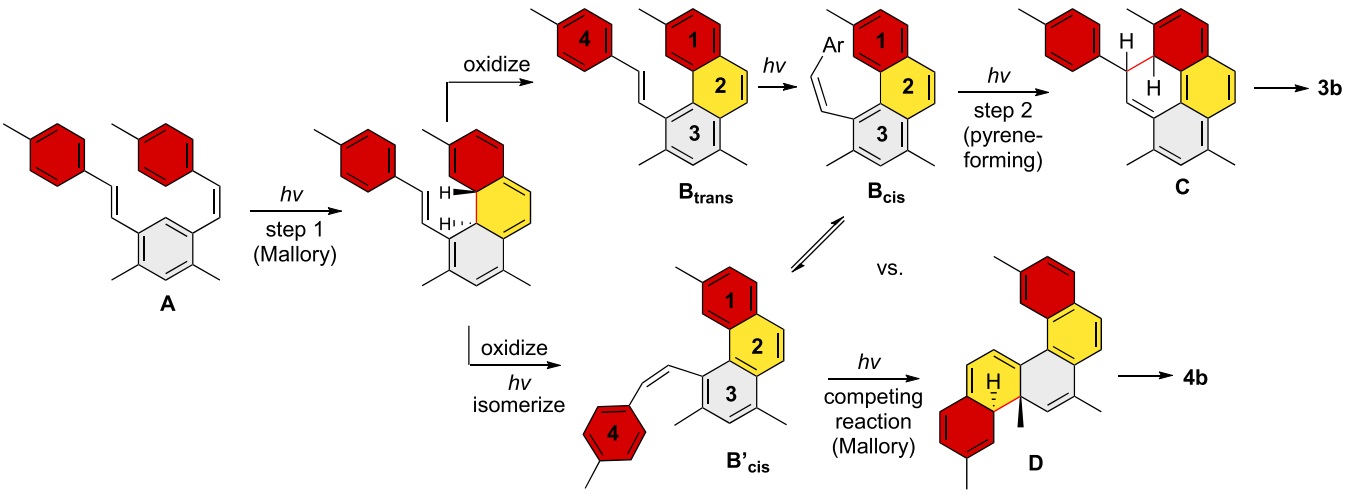

https://doi.org/10.1021/jacs.4c14486
J. Am. Chem. Soc. 2025, 147, 1074−1091

Scheme 9. Computed Reaction Profiles for (A) Pyrene-Forming vs (B) Chrysene-Forming Photocyclization Steps[a]

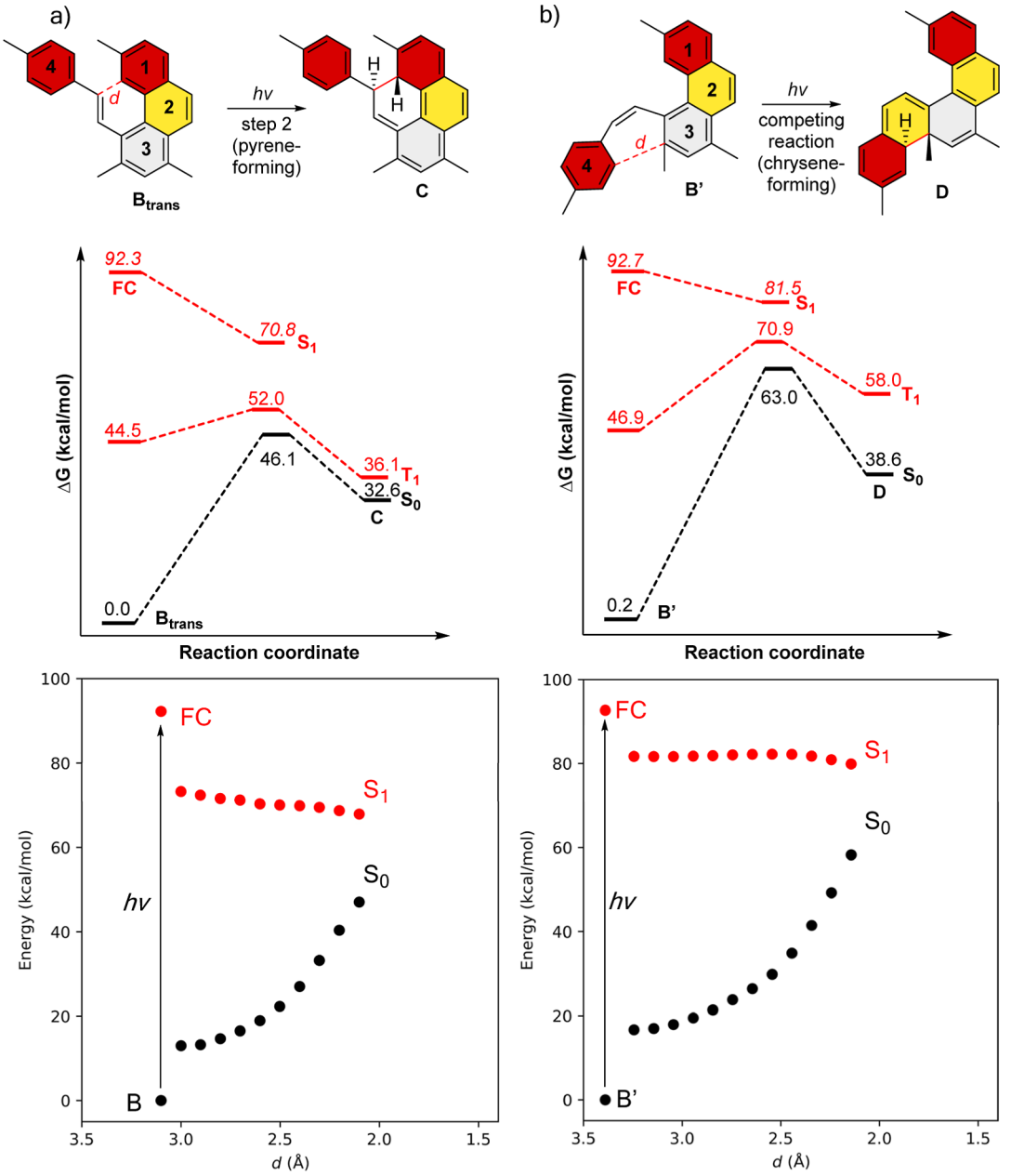

[a]Top: schematic illustration of the competing photocyclization steps. Middle: computed conrotatory electrocyclization reaction profiles in the S_0 and T_1 states. Single-point energies in the S_1 state were computed for the S_0 state minima and transition state structures. Bottom: S_1 state (red) and S_0 state (black) energy profiles were computed along the coordinate of the forming C−C bond ("*D*") at (TD-)M06-2X(D3)/6-31+G(d).

energy profile for the pyrene-forming reaction shows a modest downhill trajectory (red dots, Scheme 9a, bottom), while the chrysene-forming reaction is relatively "flat" and featureless (red dots, Scheme 9b, bottom).

In our experiments, replacing the two methyl groups on ring 3 by two H's gives rise to near exclusive chrysene products, with pyrene forming only in trace amounts. Hence, a comparison of the two substrates can be useful for understanding the observed selectivity. However, we found that the relaxed S_1 potential energy profile scans along the cyclization reaction coordinate are quite similar to the R = Me plots shown in Scheme 9. Again, a larger energy drop from the Franck−Condon point is found at the pyrene-forming path (see computed reaction profiles for R = H in the SI), despite the experimental preference for the Mallory reaction. However, a comparison of the ground-state conformations revealed an additional factor that may contribute to the observed experimental differences (Scheme 10). Computational results show that when R = H, **B′** is 0.8 kcal/mol lower in free energy than its conformational isomer $\mathbf{B}_{cis}$. This difference could contribute to the observed product selectivity according to the nonequilibration of the excited-state rotamers (NEER) principle.[73] The NEER principle describes how the ground state conformational population can dictate the outcome of photochemical reactions. When R = H, **B′** is the more accessible conformation, and thus photocyclization leads to a dominant chrysene product. However, because the observed conformational difference is relatively small, it is likely that the

https://doi.org/10.1021/jacs.4c14486
J. Am. Chem. Soc. 2025, 147, 1074−1091

Scheme 10. Computed Isotropic NICS(1) In the S_0 and T_1 States for Structures (A) B_{trans} and B_{cis} and (C, B) B′ and D at B97-2/6-311+G(d,p)//M06-2X(D3)/6-31+G(d). Blue Color and Negative NICS Values Indicate Aromaticity, Red Color and Positive NICS Values Indicate Antiaromaticity

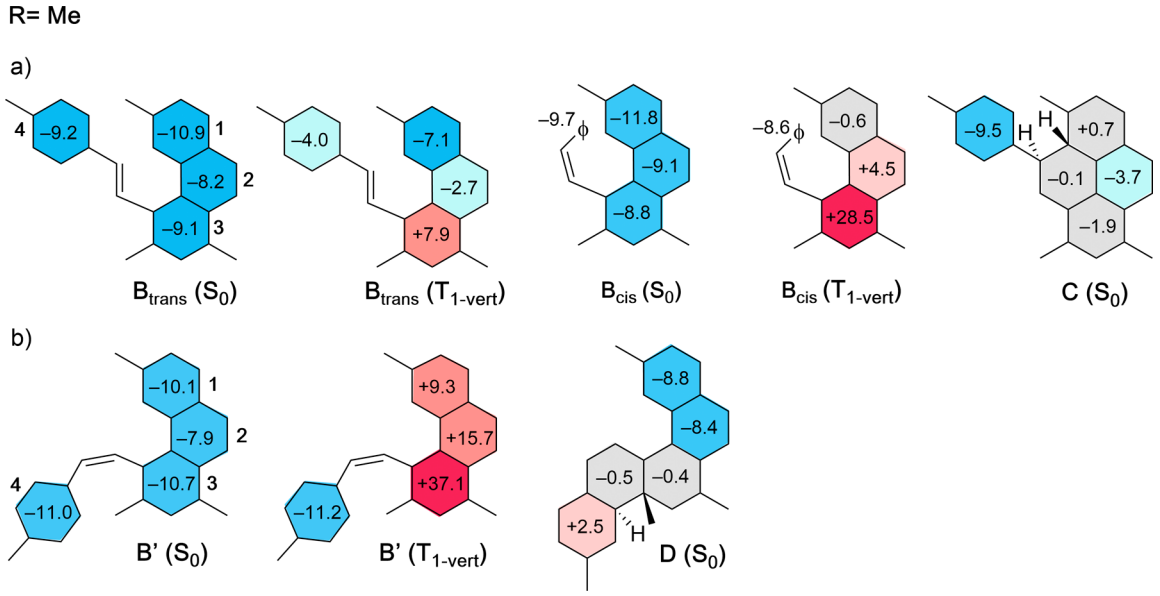

Scheme 11. Competition between 1,5 H- and 1,2 H-Shifts in Dihydrophenanthrene Formation

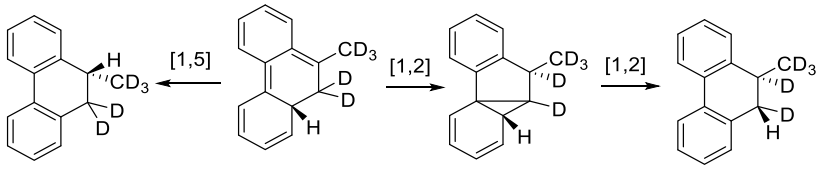

1:9 ratio for [1,5] vs [1,2] shift products *JOC*, **2005**, 10447

selectivity trends originate from a combination of more than one factor.

We also wondered if Baird's rules,[74−76] i.e., a reversal of the Hückel rule in the lowest $\pi\pi^*$ states, might play a role in triggering these sequential photocyclization reactions. Both electrocyclization reactions are challenging in the ground state due to the disruption of aromaticity upon forming either pyrene or chrysene. Indeed, computed nucleus-independent chemical shifts, NICS(1), at 1 Å above the individual ring centers of $\mathbf{B}_{trans}$, $\mathbf{B}_{cis}$, and **B′**, show large negative NICS(1) values for all of the rings in the S_0 state.[77]

Triplet state NICS computed for the S_0 geometries at the Franck−Condon point indicate that all vertically excited triplet species ($T_{1\text{-vert}}$), $\mathbf{B}_{trans}$, $\mathbf{B}_{cis}$, and **B′** show increased paratropicity (or decreased diatropicity) in the phenanthrene core. Notably, ring 3, i.e., the target for the Mallory reaction, displays the strongest paratropic character (i.e., excited-state antiaromatic) for all three structures in the vertically excited triplet state.

Upon photocyclization, intermediate **C** retains one strongly aromatic terminal aryl ring (ring 4), while intermediate **D** features an aromatic naphthalene fragment (rings 1 and 2). However, both structures display a nonaromatic ring 3, indicated by near-zero NICS(1) values. These findings suggest that, in the second photocyclization step, both the pyrene- and chrysene-forming reactions involve the relief of excited-state antiaromaticity in ring 3, as evidenced by the small NICS(1) values in both **C** and **D**. Computed NICS(1) values for the R = H analogs of $\mathbf{B}_{trans}$, $\mathbf{B}_{cis}$, and **C** as well as **B′** and **D** show qualitatively similar results (Table S21).

Mechanism: Aromatization and Migration Steps. The post-cyclization stage of this cascade also includes interesting mechanistic features related to migration and aromatization, with aromatization potentially proceeding via two distinct paths, intermolecular and intramolecular.

In the first scenario, this aromatization can occur via a sequence of intramolecular H and Ar shifts. The simplest path would include a 1,5-hydrogen shift that would directly convert the initial cyclization product **C** to the dihydropyrene product. This process is highly favorable thermodynamically (>50 kcal/mol exergonic) due to the aromatization of phenanthrene moiety embedded in the product. However, activation barriers for 1,5-shifts in rigid cyclohexadiene systems are known to be relatively high due to the significant strain in the migration transition state.[78]

The intramolecular path to aromatization is topologically identical to a process analyzed in the seminal studies of Lewis, Gevorgyan, and co-workers (Scheme 11). This earlier work investigated whether the photocyclization of vinyl-biphenyl is finalized through a 1,5 H-shift or two 1,2 H-shifts.[79] Experimental results using deuterium labeling have shown that, while at lower temperatures, the 1,5 H-shift prevails, the room temperature pathway preferred two consecutive 1,2 H shifts. Interestingly, the ground state computational barriers do not reproduce this trend, suggesting either a possible

https://doi.org/10.1021/jacs.4c14486
J. Am. Chem. Soc. 2025, 147, 1074−1091

involvement of tunneling or a scenario in which the H-shifts proceed fully or partially at the excited state surface.

Although our cyclization proceeds at a phenanthrene moiety instead of a biphenyl, the topology of the H-shifts is similar. Although the 1,5 H-shift would simultaneously aromatize two aromatic rings, the hydrogen atom would have to "skip a carbon", i.e., migrate over a methylene group confined within a rigid polycyclic hydrocarbon. On the other hand, each of the 1,2 H-shift aromatizes only one of the two rings, but the geometric constraints are much less severe since hydrogen moves only to an adjacent carbon.

Unfortunately, the nature of H atom migrations in our systems is hard to pinpoint experimentally (e.g., through the isotope effects used above) since the hydrogen atoms are lost during the subsequent "second stage" aromatization. Because the pendant Ar group can also shift in some substrates, our efforts were focused on understanding this migration as an alternative to an H-shift (Scheme 12). Energies for these

Scheme 12. Barriers for 1,2-Ar vs 1,2 H-Shift From A,B for the Me (Left) and OMe (Right) Substrates

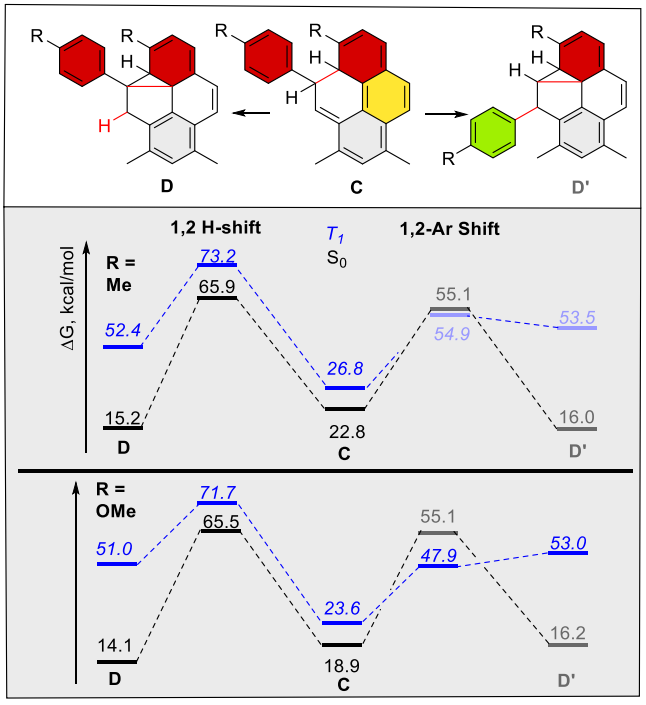

diverging scenarios (1,2 H-shift vs 1,2-Ar-shift) show that the barriers for Ar-migration are significantly lower (32−36 kcal/mol) than for the hydrogen migration (43−47 kcal/mol). However, the calculated barriers are sufficiently high to make both of these processes unlikely. The analogous shifts in the triplet excited state have similar problems. Although barriers for the Ar-shifts decreased to 24−28 kcal/mol for R = OMe, these computational results suggest that aromatization should proceed through an alternative mechanism.

Because the classic concerted H- and Ar-shifts are difficult, one has to look for an alternative. In this context, it is important to keep in mind that the Mallory reaction combines photochemical and radical steps. In particular, the Katz conditions are associated with the presence of I_2 that can dissociate into iodine atoms under photochemical conditions. Considering that assistance by radical species is a likely process. Indeed, the calculated bond dissociation energies (BDEs) show that two C−H bonds in intermediate **C** are very weak (BDE = 29 and 51 kcal/mol). Hence, the formation of strained intermediate **D** can be bypassed, and the initial cyclization product b can be converted into the pyrene product by simply losing the two H atoms in radical reactions. Furthermore, radical H atom transfer at the weakest C−H bond leads to radical **E′** with the spin density at the perfect location for promoting the observed Ar migration via a simple radical 1,2-Ar shift. This scenario provides a very simple explanation of why the Ar shift is observed for Ar = *p*-Ph-OMe. Not only does the OMe group in the migrating Ar group provide kinetic stabilization to the migrating TS but also the OMe group in the polycyclic core is at the right position to stabilize the delocalized radical in the product (Scheme 13).

Scheme 13. Weak C−H Bonds Lead to Crossover From the Photochemical-to-Radical Mechanism

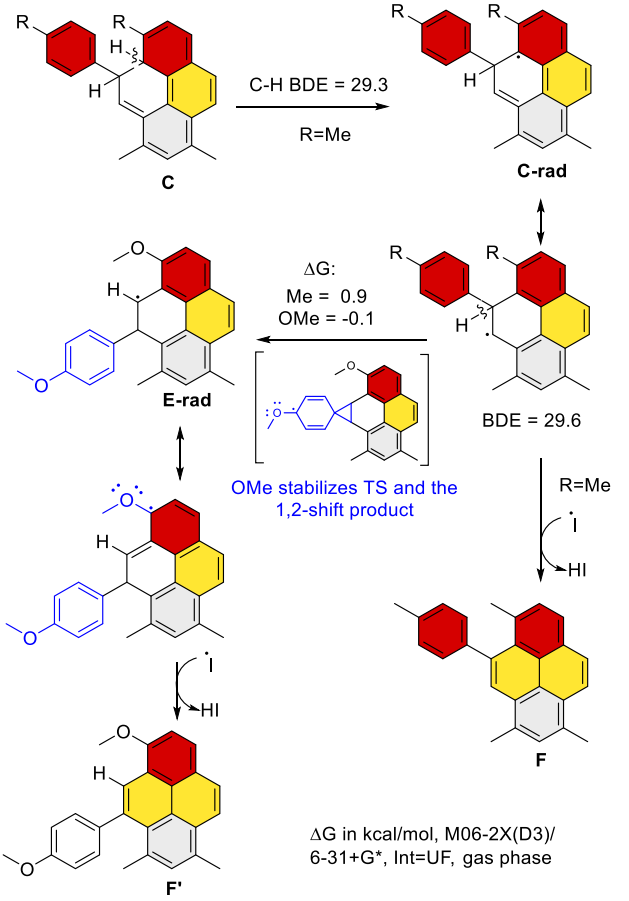

Hence, the refined mechanistic proposal emerges from the fusion of the photochemical and radical pathways. The *bis*-stilbene precursor **A** undergoes 6π-electrocyclization and oxidation to give phenanthrene **B**. Subsequent 6π-electrocyclization at the bay region of phenanthrene gives the tetracyclic core of product **C**. The salient feature of this product is the presence of a very weak C−H bond (BDE = 29 kcal/mol). Radical abstraction at this activated bond leads to a polycyclic radical that can either lose another hydrogen atom (and give product F) or undergo a 1,2-Ar shift to give the more stable radical **E-rad**. The TS for this transformation can be stabilized by the O−Me substituent in the pendant phenyl ring.

https://doi.org/10.1021/jacs.4c14486
J. Am. Chem. Soc. 2025, 147, 1074−1091

Scheme 14. Radical Mechanism Accounts for the Observed Loss of the Alkyl Blocking Groups

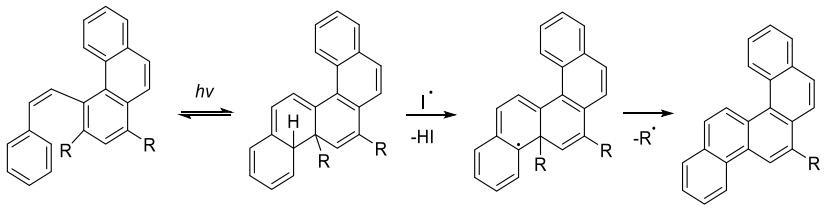

Table 1. Photophysical Properties for 50 μM Solutions of Pyrenes in CH_2Cl_2 (λ_{ex} = 360 nm)

		emission at rt				
compound	absorbance λ (nm) (ε, × 10^4 M^{-1} cm^{-1})	λ_{max} (nm)[a]	τ (ns)[b]	Φ_{PL}	k_r (× 10^6 s^{-1})[c]	k_{nr} (× 10^7 s^{-1})[d]
pyrene[e]	337 (4.8)	373	[f]	0.05		
3a	357 (4.6)	384	17.0	0.11	6.5	5.2
3d	365 (2.8)	393	4.1	0.06	14.6	22.9
3g	361 (3.2)	391	14.6	0.18	12.3	5.6
3l	361 (3.4)	391	14.6	0.19	13.0	5.6
3e	367 (4.2)	405	5.5	0.35	63.6	11.8
3o	302 (1.1)	384	4.4	0.35	79.5	14.8
3j	366 (3.2)	407	5.2	0.37	71.2	12.1
3c	364 (3.4)	393	11.5	0.20	17.4	7.0
3b	362 (3.9)	391	14.6	0.18	12.3	5.6

[a]Highest energy emission peak. [b]Acquired at the emission maximum. [c]$k_r = \Phi/\tau$. [d]$k_{nr} = (1-\Phi)/\tau$. [e]From.[37] [f]The emission decay was within our instrument response function (t < 1 ns).

Furthermore, the unpaired electron in **E-rad** can be stabilized by the OMe substituent in the core pyrene moiety. These two effects support experimental results of observed aryl migration when R = OMe vs the absence of migration when R = Me, Cl, and H. For R = *t*-Bu, migration is driven by release of steric bulk, suggesting that not only product stabilization but reactant destabilization can also be used to promote the 1,2-aryl shift.

Finally, C−H bonds next to a radical are known to be particularly weak, so the last hydrogen loss can proceed quickly to furnish the rearranged pyrene product **F′**.

Another piece of evidence supporting a radical mechanism is the observed loss of alkyl blocking groups. The driving force for the radical C−R fragmentation should increase with the stability of radical R (*t*-Bu > i-Pr > Et > Me, Scheme 14). This step, which renders the second Mallory reaction irreversible, is therefore more favorable for the more substituted radicals. This factor counterbalances the blocking group's effect on the competition between the Mallory cyclization and the "pyrene" cyclization.

Photophysics: General Trends as a Function of Substitution at the Pyrene Core. The unusual non-symmetric substitution patterns of the classic pyrene chromophore provided an opportunity to explore its photophysical properties, which we will present and discuss in this section.[80,81]

The UV spectrum of pyrene in DCM at 50 μM concentration shows the characteristic vibronic progression with peaks at 338 (λ_{max}), 321, 305, and 295 nm. The fluorescence spectrum on the other hand is dominated by five major bands between 375 and 410 nm.[82] Absorption and emission spectra of **3-e**, **3g**, **3j**, **3l**, and **3o** are mirror images with a Stokes shift of <3000 cm^{-1}. In line with previous examples[37,83] (Table 1), the incorporation of a phenyl group results in a red shift in absorption and emission (**3a** vs pyrene). The spectra are oxygen-independent, indicating emission from a singlet state.

In the earlier work from our lab, Gonzales-Rodriguez et al. found that, although pyrene has only one of the three lowest excited states allowed according to DFT calculations, non-symmetric substitutions lower these symmetry restrictions and create new low-energy excitations.[37] Overall, the introduction of substituents results in a more than 2-fold increase in emission quantum yield relative to unsubstituted pyrene (except **3d**). As suggested previously,[37] the symmetry breaking by substitution likely increases the allowedness of the S_1 to S_0 transition, resulting in an increase in k_r and consequently, the quantum yield. For the chloro-substituted complex **3d**, any increase in k_r is likely to be offset by the increase in k_{nr} (largest in the series), which results in a quantum yield similar to that of the parent pyrene. It is likely that the C−Cl moiety introduces a new vibrational relaxation mode. Comparison of **3a**, **3g**, **3l**, **3c**, and **3b** shows that the addition of a third alkyl substituent on the pyrene core further increases the quantum yield. This change can also be attributed to an increase in k_r, presumably due to the same increased symmetry breaking.

The nature of alkyl substituent (Me, Et, i-Pr) in Ph-substituted pyrenes **3g**, **3l**, **3c**, and **3b** does not greatly influence the lifetimes and quantum yields (**Φ**). This illustrates that the impact of the alkyl substituent on the electronic properties of the pyrene core and on the photophysics in dilute solutions is minimal.

However, the methoxy substituted pyrenes show a markedly different trend with the i-Pr substituted pyrene **3o** displaying photophysics that is unique in these series. First, while its emission is still red-shifted relative to pyrene itself, this shift is much less pronounced than in other methoxy substituted pyrenes. Furthermore, unlike all other substrates, the absorbance of **3o** is blue-shifted, showing 20−25% shorter emission lifetime and 12−25% higher k_r. Methoxy substituted pyrenes **3e**, **3o**, and **3j** have the highest emission quantum yields (35−37%) which can be attributed to a more than 3-fold

https://doi.org/10.1021/jacs.4c14486
J. Am. Chem. Soc. 2025, 147, 1074−1091

increase in k_r relative to the alkyl equivalents (**3g**, **3l**, **3c**, and **3b**).

We also explored the effect of 4,5,6-substitution on the photophysical trends of the pyrene moiety. For this, we analyzed absorbance and emission spectra for pyrenes **3a**–**e** with different groups in the 1,3-dimethyl pyrene core (Figure 1, top). In the absorption spectra, all these pyrenes gain a new

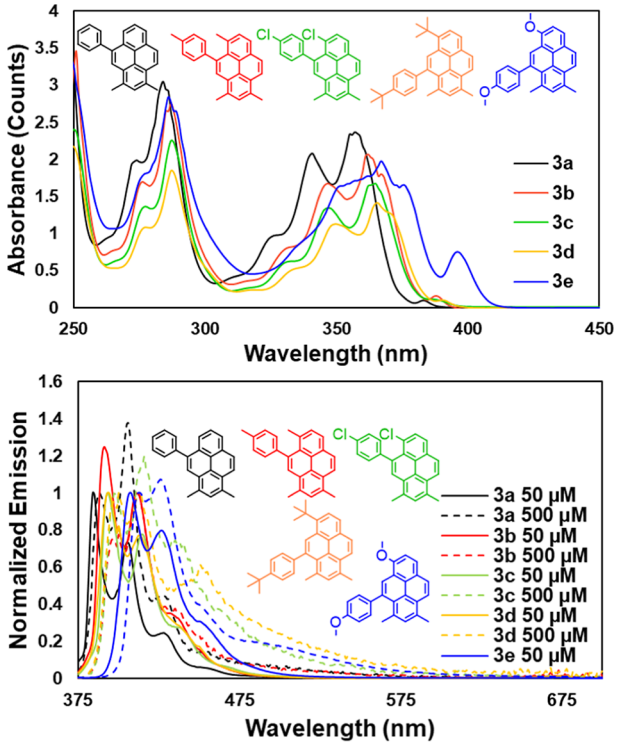

Figure 1. Absorption [50 μM] and normalized emission [50 μM and 500 μM] spectra of the 1,3-dimethyl pyrenes **3a**, **3b**, **3c**, **3d**, and **3e** in DCM.

shoulder peak at ~380–400 nm. Compounds **3b**–**d** are slightly red-shifted relative to Ph-substituted **3a**. The methoxy-substituted pyrene **3e** on the other hand does not have the classic pyrene vibronic structure and is further red-shifted. Emission spectra show similar characteristics with the typical Stokes shifts (10–50 nm). While the phenyl and tolyl pyrenes **3a,b** (Figure 1, bottom) show weak excimer formation suggested by the long red-shifted shoulder from ~475–600 nm at high concentrations (1000 μM), compounds **3c**–**e** display much more pronounced red-shifted shoulders, indicating better excited state aggregation (Figure 1, bottom). This effect comes from pyrene forming excited state dimers that emit at red-shifted wavelengths.

Next, we compared how different alkyl blocking groups R affect the absorbance and emission properties of tolyl-substituted pyrenes (Figure 2). Although the absorbance spectra are nearly identical, the emission spectra show a more interesting trend (Figure 2, top). As this trend is only apparent at higher concentrations, it has to reflect the differences in aggregation properties. As the concentration increases from 50 to 500 μM, the spectrum of i-Pr pyrene **3l** starts to show the signs of excimer formation which are not present in the Me-substituted pyrene **3b**. However, both of these compounds behave drastically differently from the Et-substituted pyrene **3g**, where the appearance of a new broad red-shifted band

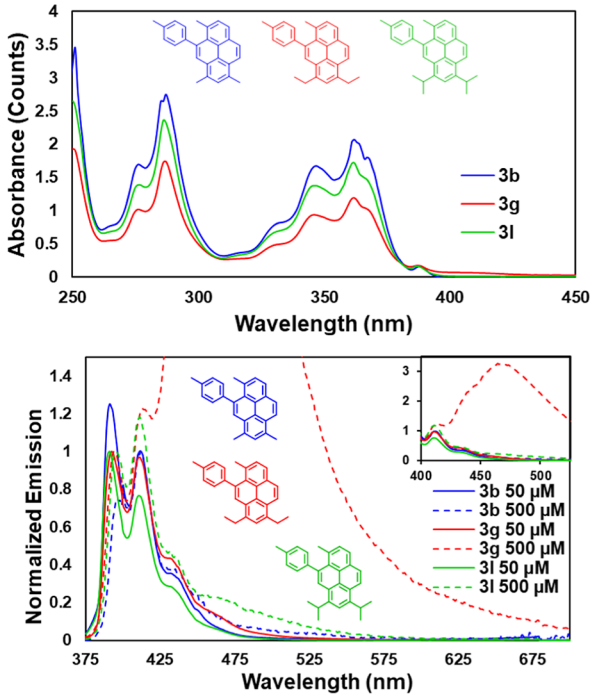

Figure 2. Absorption [50 μM] and normalized emission [50 μM and 500 μM] spectra of **3b**, **3g**, and **3l** in DCM.

centering at ~475 nm and extending beyond 700 nm completely overshadows its single molecule emission (Figure 2, bottom).

The growth of a broad emission peak at 450–550 nm with increasing concentration of **3a,b,e, g**, is consistent with the known excimer emission from pyrene compounds.[84] Time-resolved emission for the low energy feature exhibits a rise in the first 5 ns, followed by decay, which is consistent with diffusion-limited pyrene excimer behavior.[85] In **3a**, **3e,** and **3b**, it is less pronounced than monomer emission even at 500 mM, but for **3g**, it becomes the dominant emission at >250 mM. Apparently, while Me and i-Pr blocking groups are either too small or too big, the Et blocking group creates the perfect alignment for excited state aggregation and excimer emission.

An even more surprising observation comes from the absorbance and emission spectra of anisyl-substituted pyrenes (R′ = OMe, Figure 3). For the Me and Et blocking groups, the absorbance spectra are almost identical, showing a peak at ~400 nm (Figure 3, top). Pyrene **3o**, on the other hand, has an absorption spectrum that is different from that of all other pyrenes discussed in this work. It features only a single blue-shifted peak at ~305 nm. The differences in the emission spectra are less pronounced but still apparent (Figure 3, bottom). At the higher concentration, Me-pyrene **3e** displays excimer emission at ~500 nm. The same, albeit weaker, feature is also seen in Et-pyrene **3j**. For these two anisyl-substituted pyrenes, excited state aggregation decreases as blocking group size increases. The i-Pr pyrene **3o** shows identical emissions at both low and high concentrations, indicating the lack of light–driven complex formation.

Overall, the observed behavior is quite diverse with certain molecules (e.g., **3g** and **3o**) displaying distinctly different features. To probe the origin of these variations deeper, we conducted an additional computational study of the unusual behavior of pyrene **3o**, which is detailed below.

https://doi.org/10.1021/jacs.4c14486
J. Am. Chem. Soc. 2025, 147, 1074–1091

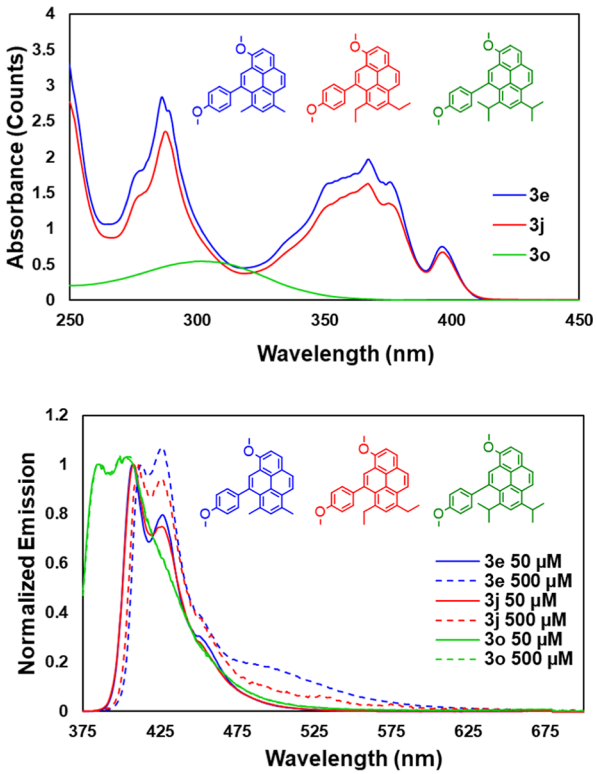

Figure 3. Absorption [50 μM] and normalized emission [50 μM and 500 μM] spectra of **3e**, **3j**, **3o** in DCM.

Photophysical Puzzle: Differences in the Absorbance Spectra of 3e vs 3o. While **3e** exhibits an absorbance spectrum similar to that previously reported for nonsymmetric pyrenes, the spectrum for **3o** is blue-shifted and shows a single, broadened peak (Scheme 15). Computed spectra for monomers of **3e** and **3o**, at the TD-M06-2X(D3)/def2-SVP level, show two broad peaks, at the 225−260 and 320−340 nm regions, consistent with the observed absorption spectrum for **3e**. However, stacked dimers and tetramers of **3e** and **3o** show only a single broad peak in the 330−340 nm region, similar to the observed spectrum for **3o** (see the Supporting Information, Figures S60−S64). This comparison suggests that the single broad peak observed for **3o** may be associated with aggregation.

Tetramers of H-aggregates were computed to compare the stacking interaction energies of **3e** vs **3o**. Averaged interaction energies (ΔG_{int}) were calculated at M06-2X(D3)/def2-SVP based on the energy difference between the tetramer and four times the energy of a monomer, then divided by three; $\Delta G_{int} = (G_{tetramer}) - (G_{monomer} \times 4)/3$. Computed H-aggregate models revealed weaker stacking interactions for **3e** (ΔG_{int} = 8.9 kcal mol^{-1}) and stronger interactions for **3o** (ΔG_{int} = 13.1 kcal mol^{-1}) (Figure S62), which may be attributed to dispersion interactions between the bulky blocking groups in **3o**. We also notice that **3e** and **3o** are stacked slightly differently: **3e** is slip-stacked horizontally along the *x*-axis, while **3o** is slip-stacked vertically along the *y*-axis (Figure S61).

J-aggregate tetramers were also computed, but the averaged interaction energies were both relatively low and nearly identical (ΔG_{int} = 9.5 kcal mol^{-1} for **3e** and ΔG_{int} = 9.5 kcal mol^{-1} for **3o**, see Figure S62, bottom). The potential formation of H-aggregates of **3o** is further supported by a large k_r value, as H-aggregates are known to be not only blue-shifted but also more emissive.[86] Indeed, **3o** has the highest k_r among all of the compounds in Table 1.

Scheme 15. Top: Difference in Absorbance Reflect Changes in Excited States in Pyrene as a Function of Substitutions[a]

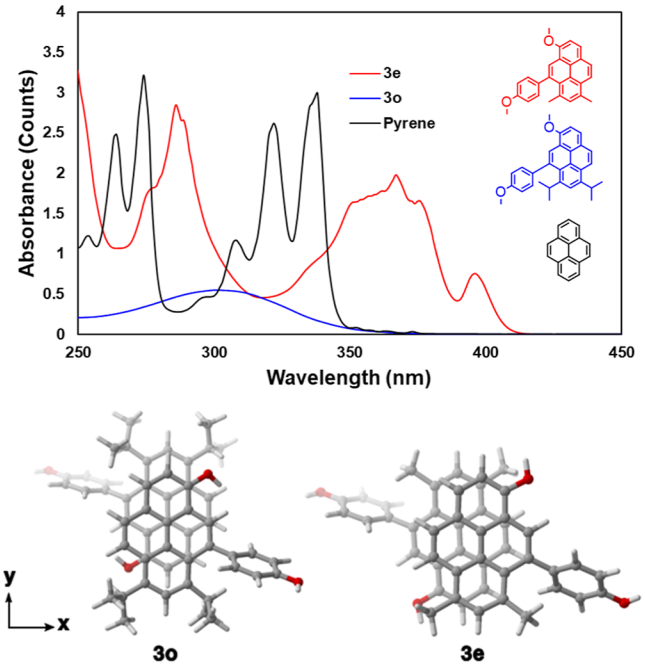

[a]Absorbances taken at 50 μm. Bottom: optimized dimer geometries for **3e** and **3o**.

CONCLUSIONS

Hundreds of literature examples of 6π-electrocyclic ring closure in stilbenes (the Mallory cyclization) provide a drastic contrast to the surprising scarcity of similar 6π-electrocyclic closures in the bay region of phenanthrenes. It was even stated in the literature that this oxidative photocyclization should be impossible.[60,87] The present work fills this gap by showing that this photochemical cyclization is viable, expanding the list of alternatives to the classic Mallory path.[88]

The new photochemical cascade reported in this work diverts the photochemistry of *bis*-stilbenes from the double Mallory cyclization toward the formation of nonsymmetrical pyrenes. The competition between the Mallory reaction and the previously unknown alkene cyclization at the phenanthrene bay region can be controlled by installing alkyl groups to avoid the undesired Mallory cyclization.

DFT computations illustrate the role of photochemical excitation in the observed cyclization steps. Analysis of local aromaticity in the existing and forming rings reveals that escape from excited-state antiaromaticity facilitates both the Mallory and the "pyrene" cyclization steps (Scheme 16). In both cases, one of the rings becomes strongly antiaromatic in the vertically excited state, but this electronic feature is transient and antiaromaticity is fully relieved by alkene twisting. Antiaromaticity relief has important consequences for both cyclization steps. The same geometric change that restores aromaticity in the pre-existing rings also activates alkene for the cyclization step. Such activation of alkenes with aromatic substituents seems to be a general feature of their photochemistry.[89−95]

https://doi.org/10.1021/jacs.4c14486
J. Am. Chem. Soc. 2025, 147, 1074−1091

Scheme 16. Selected Photocyclization Patterns (Colors Denote Aromaticity Patterns for the Vertical T1 States)

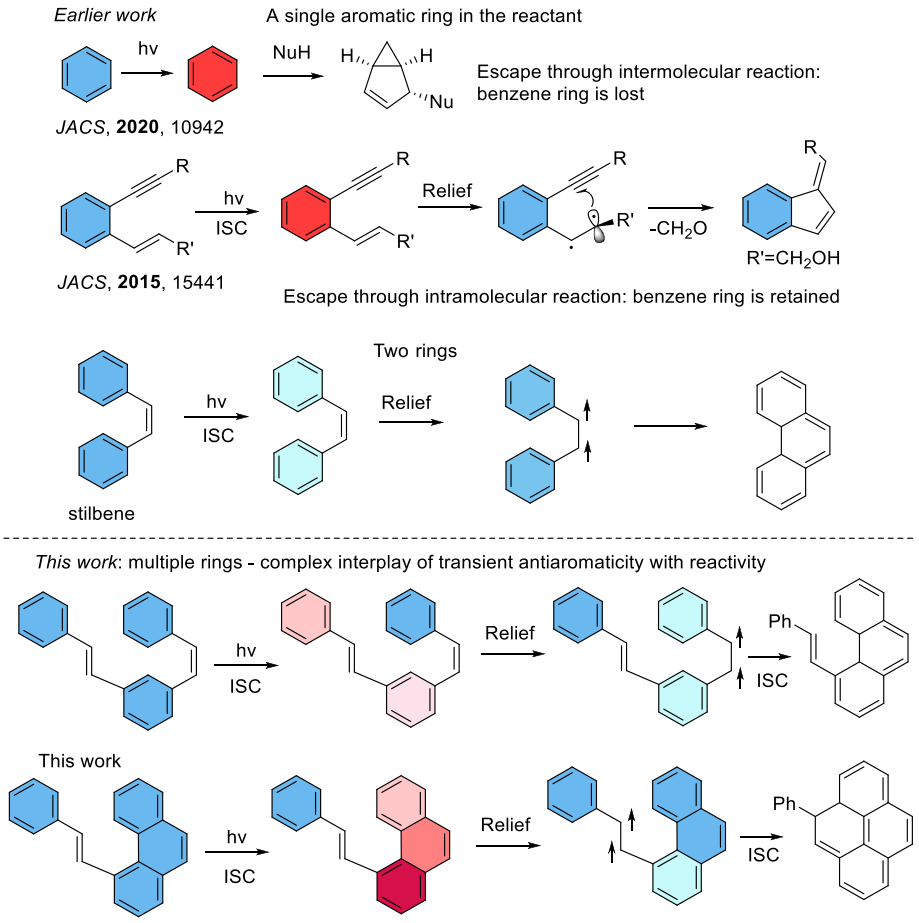

Interestingly, the vertical excited state of phenanthrene is much more antiaromatic than that of stilbene. From that point of view, one can argue that the "pyrene" cyclization gets a larger boost from transient antiaromaticity than from the Mallory cyclization. However, both reactions show transient formation of antiaromatic regions followed by their dissipation/rearomatization but with triplet character moving to the alkene parts. The localized triplet state on alkenes can be considered "hot spots" that promote the ring-forming processes.[46]

DFT computations also suggest that although a reversal of aromatic and antiaromatic character in the excited state is key to triggering this photochemical cascade, many features of the excited state potential energy combine in controlling the product selectivity. Photocyclization reactions for competing pyrene-forming vs chrysene pathways are barrierless in the S_1 state but can be influenced by (1) the steepness descent from the Franck−Condon region toward the cyclization reaction coordinate or by (2) ground state conformational population following the NEER principle.[96,97] Furthermore, the cyclization steps are reversible, as the products are much higher in energy than the ground-state starting materials. Hence, one can consider these to be, in essence, photochromic systems, where the cyclic product needs to be trapped to prevent the ring opening. Differences in the efficiency of such trapping steps can also contribute to the observed selectivity.

This work also illustrates that synthetically useful photochemistry can occur under mechanistically complex conditions where photo- and radical reactions coexist and depend on each other. An interesting crossover between photo- and radical chemistry occurs under the classic Katz conditions, where dehydrogenation of the initially formed dihydrophenanthrene intermediate is promoted by the presence of I_2. This crossover has two mechanistically and practically interesting consequences: an interesting one, i.e., the extension of cascade via radical migration of electron-rich aryl groups, and an unfortunate one, i.e., the possibility of radical C−C scissions that remove the blocking alkyls and reopen the doors for the Mallory path. The latter observation reiterates the lability of C−C bonds in radical processes, especially when aromatization is possible.[47,93,98−106]

Still, even though engineering excited state reactivity is challenging, this work shows that rational design (i.e., the use of blocking groups) allows one to control a classic photochemical process (the Mallory cyclization). Depending on the chemist's will, it can be allowed to proceed as expected at the beginning or prevented at a later stage of the photochemical cascade.

The new nonsymmetric pyrenes present unique opportunities for excited state engineering, particularly through their lower symmetry excited states and the pronounced impact of subtle structural changes on excimer formation. For example, the size of the alkyl groups imposes irregular effects. In particular, excimers are not formed when pyrene substituents are too small (Me) or too large (i-Pr) but appear for a substituent of an intermediate size (Et). In contrast, when an additional R′ = OMe is introduced, excimer formation increases as the alkyl group size transitions from R = Me to

https://doi.org/10.1021/jacs.4c14486
J. Am. Chem. Soc. 2025, 147, 1074−1091

R = i-Pr. Furthermore, the unusual behavior of pyrene **3o** suggests high-level ground state supramolecular preorganization. Even before the photon is absorbed, these pyrenes are already self-assembled. These results illustrate the new possibilities of precise supramolecular control and excited state engineering in this classic chromophore.

■ ASSOCIATED CONTENT

Supporting Information

The Supporting Information is available free of charge at https://pubs.acs.org/doi/10.1021/jacs.4c14486.

Experimental procedures, analytical data (^{1}H and ^{13}C NMR and MS) for all new compounds as well as optimization tables; UV−vis absorption and emission spectra of the new pyrenes; details of X-ray crystallographic analysis and geometric parameters of pyrenes; and Cartesian coordinates and energies for optimized S_0 and S_1 geometries of reactants and intermediates (PDF)

Accession Codes

Deposition Numbers 2258105, 2291425, 2309513, 2391365−2391371, and 2391375 contain the supplementary crystallographic data for this paper. These data can be obtained free of charge via the joint Cambridge Crystallographic Data Centre (CCDC) and Fachinformationszentrum Karlsruhe Access Structures service.

■ AUTHOR INFORMATION

Corresponding Authors

Judy Wu − *Department of Chemistry, University of Houston, Houston, Texas 77204, United States;* orcid.org/0000-0003-0590-5290; Email: jiwu@central.uh.edu

Igor V. Alabugin − *Department of Chemistry and Biochemistry, Florida State University, Tallahassee, Florida 32306, United States;* orcid.org/0000-0001-9289-3819; Email: alabugin@chem.fsu.edu

Authors

Nikolas R. Dos Santos − *Department of Chemistry and Biochemistry, Florida State University, Tallahassee, Florida 32306, United States;* orcid.org/0009-0004-6394-0945

João Vitor Schober − *Department of Chemistry, University of Houston, Houston, Texas 77204, United States;* orcid.org/0000-0002-7070-8376

Croix J. Laconsay − *Department of Chemistry, University of Houston, Houston, Texas 77204, United States;* orcid.org/0000-0002-9244-1318

Alexandria M. Palazzo − *Department of Chemistry and Biochemistry, Florida State University, Tallahassee, Florida 32306, United States*

Leah Kuhn − *Department of Chemistry and Biochemistry, Florida State University, Tallahassee, Florida 32306, United States*

Angel Chu − *Department of Chemistry and Biochemistry, Florida State University, Tallahassee, Florida 32306, United States*

Benjamin Hanks − *Department of Chemistry and Biochemistry, Florida State University, Tallahassee, Florida 32306, United States;* orcid.org/0009-0009-1158-2353

Kenneth Hanson − *Department of Chemistry and Biochemistry, Florida State University, Tallahassee, Florida 32306, United States;* orcid.org/0000-0001-7219-7808

Complete contact information is available at: https://pubs.acs.org/10.1021/jacs.4c14486

Notes

The authors declare no competing financial interest.

■ ACKNOWLEDGMENTS

We are grateful to the National Science Foundation (NSF) for financial support (CHE-2102579). We would also like to acknowledge Florida State University for providing facilities and equipment used to complete this research. This work made use of the Rigaku Synergy-S single-crystal X-ray diffractometer that was acquired through the NSF MRI program (award CHE-1828362) and used with the help of Dr. Xinsong Lin. The authors are also thankful to the FSU NMR facility and Dr. Banghao Chen (FSU075000NMR). J. I. W. thanks the National Institute of General Medical Sciences (NIGMS) of the National Institutes of Health (R35GM133548) and the Alfred P. Sloan Research Foundation (FG-2020-12811) for funding support. We acknowledge the use of the Carya and Sabine clusters and support from the Research Computing Data Core at the University of Houston.

■ REFERENCES

(1) Anant, P.; Lucas, N. T.; Ball, J. M.; Anthopoulos, T. D.; Jacob, J. Synthesis and Characterization of Pyrene-Centered Oligothiophenes. *Synth. Met.* **2010**, *160* (17), 1987−1993.

(2) Wu, J.; Pisula, W.; Müllen, K. Graphenes as Potential Material for Electronics. *Chem. Rev.* **2007**, *107* (3), 718−747.

(3) Vögtle, F.; Neumann, P. Stereochemistry of [2.2]-Metacyclophanes. *Angew. Chem., Int. Ed. Engl.* **1972**, *11* (2), 73−83.

(4) Kawano, S.; Yang, C.; Ribas, M.; Baluschev, S.; Baumgarten, M.; Müllen, K. Blue-Emitting Poly(2,7-Pyrenylene)s: Synthesis and Optical Properties. *Macromolecules* **2008**, *41* (21), 7933−7937.

(5) Ohmori, S.; Ito, S.; Yamamoto, M. Excimer Formation and Energy Trapping in Langmuir-Blodgett Films of Poly(Vinyl Octal) Containing Pyrene Chromophore. *Macromolecules* **1990**, *23* (18), 4047−4053.

(6) Cho, H.; Lee, S.; Cho, N. S.; Jabbour, G. E.; Kwak, J.; Hwang, D.-H.; Lee, C. High-Mobility Pyrene-Based Semiconductor for Organic Thin-Film Transistors. *ACS Appl. Mater. Interfaces* **2013**, *5* (9), 3855−3860.

(7) Gong, Y.; Zhan, X.; Li, Q.; Li, Z. Progress of Pyrene-Based Organic Semiconductor in Organic Field Effect Transistors. *Sci. China:Chem.* **2016**, *59* (12), 1623−1631.

(8) Anthony, J. E. The Larger Acenes: Versatile Organic Semiconductors. *Angew. Chem., Int. Ed.* **2008**, *47* (3), 452−483.

(9) Shirota, Y.; Kageyama, H. Charge Carrier Transporting Molecular Materials and Their Applications in Devices. *Chem. Rev.* **2007**, *107* (4), 953−1010.

(10) Diring, S.; Camerel, F.; Donnio, B.; Dintzer, T.; Toffanin, S.; Capelli, R.; Muccini, M.; Ziessel, R. Luminescent Ethynyl−Pyrene Liquid Crystals and Gels for Optoelectronic Devices. *J. Am. Chem. Soc.* **2009**, *131* (50), 18177−18185.

(11) Zöphel, L.; Beckmann, D.; Enkelmann, V.; Chercka, D.; Rieger, R.; Müllen, K. Asymmetric Pyrene Derivatives for Organic Field-Effect Transistors. *Chem. Commun.* **2011**, *47* (24), 6960.

(12) Zhang, H.; Wang, Y.; Shao, K.; Liu, Y.; Chen, S.; Qiu, W.; Sun, X.; Qi, T.; Ma, Y.; Yu, G.; Su, Z.; Zhu, D. Novel Butterfly Pyrene-Based Organic Semiconductors for Field Effect Transistors. *Chem. Commun.* **2006**, No. 7, 755.

(13) Moggia, F.; Videlot-Ackermann, C.; Ackermann, J.; Raynal, P.; Brisset, H.; Fages, F. Synthesis and Thin Film Electronic Properties of Two Pyrene-Substituted Oligothiophene Derivatives. *J. Mater. Chem.* **2006**, *16* (24), 2380.

(14) Wang, Y.; Wang, H.; Liu, Y.; Di, C.; Sun, Y.; Wu, W.; Yu, G.; Zhang, D.; Zhu, D. 1-Imino Nitroxide Pyrene for High Performance

Organic Field-Effect Transistors with Low Operating Voltage. *J. Am. Chem. Soc.* **2006**, *128* (40), 13058−13059.
(15) Ashizawa, M.; Yamada, K.; Fukaya, A.; Kato, R.; Hara, K.; Takeya, J. Effect of Molecular Packing on Field-Effect Performance of Single Crystals of Thienyl-Substituted Pyrenes. *Chem. Mater.* **2008**, *20* (15), 4883−4890.
(16) Jia, W.-L.; McCormick, T.; Liu, Q.-D.; Fukutani, H.; Motala, M.; Wang, R.-Y.; Tao, Y.; Wang, S. Diarylamino Functionalized Pyrene Derivatives for Use in Blue OLEDs and Complex Formation. *J. Mater. Chem.* **2004**, *14* (22), 3344.
(17) Karuppannan, S.; Chambron, J.-C. Supramolecular Chemical Sensors Based on Pyrene Monomer−Excimer Dual Luminescence. *Chem. - Asian J.* **2011**, *6* (4), 964−984.
(18) Figueira-Duarte, T. M.; Müllen, K. Pyrene-Based Materials for Organic Electronics. *Chem. Rev.* **2011**, *111* (11), 7260−7314.
(19) Wu, J.; Zou, Y.; Li, C.; Sicking, W.; Piantanida, I.; Yi, T.; Schmuck, C. A Molecular Peptide Beacon for the Ratiometric Sensing of Nucleic Acids. *J. Am. Chem. Soc.* **2012**, *134* (4), 1958−1961.
(20) Bernhardt, S.; Kastler, M.; Enkelmann, V.; Baumgarten, M.; Müllen, K. Pyrene as Chromophore and Electrophore: Encapsulation in a Rigid Polyphenylene Shell. *Chem. - Eur. J.* **2006**, *12* (23), 6117−6128.
(21) Coventry, D. N.; Batsanov, A. S.; Goeta, A. E.; Howard, J. A. K.; Marder, T. B.; Perutz, R. N. Selective Ir-Catalysed Borylation of Polycyclic Aromatic Hydrocarbons: Structures of Naphthalene-2,6-Bis(Boronate), Pyrene-2,7-Bis(Boronate) and Perylene-2,5,8,11-Tetra(Boronate) Esters. *Chem. Commun.* **2005**, No. 16, 2172.
(22) Altschuler, L.; Berliner, E. Rates of Bromination of Polynuclear Aromatic Hydrocarbons [1]. *J. Am. Chem. Soc.* **1966**, *88* (24), 5837−5845.
(23) Dewar, M. J. S.; Dennington, R. D. DEWAR-PI Study of Electrophilic Substitution in Selected Polycyclic Fluoranthene Hydrocarbons. *J. Am. Chem. Soc.* **1989**, *111* (11), 3804−3808.
(24) Hu, J.; Zhang, D.; Harris, F. W. Ruthenium(III) Chloride Catalyzed Oxidation of Pyrene and 2,7-Disubstitued Pyrenes: An Efficient, One-Step Synthesis of Pyrene-4,5-Diones and Pyrene-4,5,9,10-Tetraones. *J. Org. Chem.* **2005**, *70* (2), 707−708.
(25) Streitwieser, A.; Lawler, R. G.; Schwaab, D. On the Bromopyrenes1. *J. Org. Chem.* **1965**, *30* (5), 1470−1473.
(26) Yamato, T.; Fujimoto, M.; Miyazawa, A.; Matsuo, K. Selective Preparation of Polycyclic Aromatic Hydrocarbons. Part 5.1 Bromination of 2,7-Di-Tert-Butylpyrene and Conversion into Pyrenoquinones and Their Pyrenoquinhydrones. *J. Chem. Soc., Perkin* **1997**, *1* (8), 1201−1208.
(27) Merner, B. L.; Dawe, L. N.; Bodwell, G. J. 1,1,8,8-Tetramethyl[8](2,11)Teropyrenophane: Half of an Aromatic Belt and a Segment of an (8,8) Single-Walled Carbon Nanotube. *Angew. Chem., Int. Ed.* **2009**, *48* (30), 5487−5491.
(28) Yang, Y.; Mannion, M. R.; Dawe, L. N.; Kraml, C. M.; Pascal, R. A.; Bodwell, G. J. Synthesis, Crystal Structure, and Resolution of [10](1,6)Pyrenophane: An Inherently Chiral [n]Cyclophane. *J. Org. Chem.* **2012**, *77* (1), 57−67.
(29) Allinger, N. L.; Gorden, B. J.; Hu, S.-E.; Ford, R. A. Some Chemistry of Compounds Related to [2.2]Metacyclophane. *J. Org. Chem.* **1967**, *32* (7), 2272−2278.
(30) Umemoto, T.; Kawashima, T.; Sakata, Y.; Misumi, S. Layered Compounds. XXV. Peropyrene and Teropyrene -a New Synthetic Route of Pyrene-like Polynuclear Aromatic Hydrocarbons-. *Tetrahedron Lett.* **1975**, *16* (12), 1005−1006.
(31) Yao, T.; Yu, H.; Vermeij, R. J.; Bodwell, G. J. Nonplanar aromatic compounds. Part 10: A strategy for the synthesis of aromatic belts-all wrapped up or down the tubes? *Pure Appl. Chem.* **2008**, *80* (3), 533−546.
(32) Laarhoven, W. H.; Cuppen, T. J. H. M. Photodehydrocyclizations in Stilbene-like Compounds. Part V. Photochemistry of 2,2′-Distyrylbiphenyl. *J. Chem. Soc., Perkin* **1972**, *1* (0), 1972−2074.
(33) Laarhoven, W. H.; Cuppen, T. J. H. M. Chiral Solvent-Induced Asymmetric Synthesis. Part 2. Photosynthesis of Optically Enriched Hexahelicenes. *J. Chem. Soc., Perkin Trans.* **1978**, *2* (4), 315−318.
(34) Padwa, A.; Doubleday, C.; Mazzu, A. Photocyclization Reactions of Substituted 2,2'-Divinylbiphenyl Derivatives. *J. Org. Chem.* **1977**, *42* (20), 3271−3279.
(35) Wang, Z. Y.; Zhang, C. Intramolecular Cyclization of 2,2'-Dibenzoylbiphenyl Units as a New Route to Increase the Rigidity and Solvent Resistance in Poly(Arylene Ethers). *Macromolecules* **1992**, *25* (21), 5851−5854.
(36) Walker, D. B.; Howgego, J.; Davis, A. P. Synthesis of Regioselectively Functionalized Pyrenes via Transition-Metal-Catalyzed Electrocyclization. *Synthesis* **2010**, *2010* (21), 3686−3692.
(37) Gonzalez-Rodriguez, E.; Abdo, M. A.; dos Passos Gomes, G.; Ayad, S.; White, F. D.; Tsvetkov, N. P.; Hanson, K.; Alabugin, I. V. Twofold π-Extension of Polyarenes via Double and Triple Radical Alkyne Peri-Annulations: Radical Cascades Converging on the Same Aromatic Core. *J. Am. Chem. Soc.* **2020**, *142* (18), 8352−8366.
(38) Wu, X.; Shi, G. Synthesis of a Carboxyl-Containing Conducting Oligomer and Non-Covalent Sidewall Functionalization of Single-Walled Carbon Nanotubes. *J. Mater. Chem.* **2005**, *15* (18), 1833.
(39) Casas-Solvas, J. M.; Howgego, J. D.; Davis, A. P. Synthesis of Substituted Pyrenes by Indirect Methods. *Org. Biomol. Chem.* **2014**, *12* (2), 212−232.
(40) Bam, R.; Yang, W.; Longhi, G.; Abbate, S.; Lucotti, A.; Tommasini, M.; Franzini, R.; Villani, C.; Catalano, V. J.; Olmstead, M. M.; Chalifoux, W. A. Four-Fold Alkyne Benzannulation: Synthesis, Properties, and Structure of Pyreno[a]Pyrene-Based Helicene Hybrids. *Org. Lett.* **2019**, *21* (21), 8652−8656.
(41) Malone, R. J.; Spengler, J.; Carmichael, R. A.; Ngo, K.; Würthner, F.; Chalifoux, W. A. Synthesis and Properties of Achiral and Chiral Dipyrenoheteroles and Related Compounds. *Org. Lett.* **2023**, *25* (1), 226−230.
(42) Yang, W.; Longhi, G.; Abbate, S.; Lucotti, A.; Tommasini, M.; Villani, C.; Catalano, V. J.; Lykhin, A. O.; Varganov, S. A.; Chalifoux, W. A. Chiral Peropyrene: Synthesis, Structure, and Properties. *J. Am. Chem. Soc.* **2017**, *139* (37), 13102−13109.
(43) Yang, W.; Chalifoux, W. A. Rapid π-Extension of Aromatics via Alkyne Benzannulations. *Synlett* **2017**, *28*, 625−632.
(44) Kawade, R. K.; Hu, C.; Dos Santos, N. R.; Watson, N.; Lin, X.; Hanson, K.; Alabugin, I. V. Phenalenannulations: Three-Point Double Annulation Reactions That Convert Benzenes into Pyrenes. *Angew. Chem., Int. Ed.* **2020**, *59* (34), 14352−14357.
(45) Morgan, D. D.; Horgan, S. W.; Orchin, M. Photocyclization of Stilbene Analogs I. The Oxidative Photocyclization of 1,3-Distyrylbenzene. *Tetrahedron Lett.* **1970**, *11* (49), 4347−4350.
(46) Zhou, Z.; Egger, D. T.; Hu, C.; Pennachio, M.; Wei, Z.; Kawade, R. K.; Üngör, O.··; Gershoni-Poranne, R.; Petrukhina, M. A.; Alabugin, I. V. Localized Antiaromaticity Hotspot Drives Reductive Dehydrogenative Cyclizations in Bis- and Mono-Helicenes. *J. Am. Chem. Soc.* **2022**, *144* (27), 12321−12338.
(47) Barton, D. H. R.; McCombie, S. W. A New Method for the Deoxygenation of Secondary Alcohols. *J. Chem. Soc., Perkin* **1975**, *1* (16), 1574−1585.
(48) Laarhoven, W. H.; Cuppen, Th. J. H. M.; Nivard, R. J. F. Photodehydrocyclizations in Stilbene-like Compounds—II: Photochemistry of Distyrylbenzenes. *Tetrahedron* **1970**, *26* (4), 1069−1083.
(49) Mallory, F. B.; Wood, C. S.; Gordon, J. T. Photochemistry of Stilbenes. III. Some Aspects of the Mechanism of Photocyclization to Phenanthrenes. *J. Am. Chem. Soc.* **1964**, *86* (15), 3094−3102.
(50) Woning, J.; Oudenampsen, A.; Laarhoven, W. H. Photochemical Addition of Methanol to Stilbenes. *J. Chem. Soc., Perkin Trans.* **1989**, *2* (12), 2147−2154.
(51) Wood, C. S.; Mallory, F. B. Photochemistry of Stilbenes. IV. Preparation of Substituted Phenanthrenes[1a−c]. *J. Org. Chem.* **1964**, *29*, 3373−3377.
(52) Noller, K.; Kosteyn, F.; Meier, H. Photochemie elektronenreicher 1,3-Distyrylbenzole. *Chem. Ber.* **1988**, *121* (9), 1609−1615.
(53) Jørgensen, K. B. Photochemical Oxidative Cyclisation of Stilbenes and Stilbenoids—The Mallory-Reaction. *Molecules* **2010**, *15* (6), 4334−4358.

https://doi.org/10.1021/jacs.4c14486
J. Am. Chem. Soc. 2025, 147, 1074−1091

(54) Meier, H. The Photochemistry of Stilbenoid Compounds and Their Role in Materials Technology. *Angew. Chem., Int. Ed. Engl.* **1992**, *31* (11), 1399−1420.
(55) Tominaga, Y.; Castle, R. N. Photocyclization of Aryl- and Heteroaryl-2-Propenoic Acid Derivatives. Synthesis of Polycyclic Heterocycles. *J. Heterocycl. Chem.* **1996**, *33* (3), 523−538.
(56) Hammond, G. S.; Saltiel, J. Photosensitized Cis-Trans Isomerization of the Stilbenes. *J. Am. Chem. Soc.* **1962**, *84* (24), 4983−4984.
(57) Saltiel, J.; Megarity, E. D.; Kneipp, K. G. The Mechanism of Direct Cis-Trans Photoisomerization of the Stilbenes. *J. Am. Chem. Soc.* **1966**, *88* (10), 2336−2338.
(58) Saltiel, J.; Zafiriou, O. C.; Megarity, E. D.; Lamola, A. A. Tests of the Singlet Mechanism for Cis-Trans Photoisomerization of the Stilbenes. *J. Am. Chem. Soc.* **1968**, *90* (17), 4759−4760.
(59) Saltiel, J.; Sun, Y. P. The Intrinsic Potential Energy Barrier for Twisting in the Trans-Stilbene S1 State in Hydrocarbon Solvents. *J. Phys. Chem.* **1989**, *93* (93), 6246−6250.
(60) Mallory, F. B.; Mallory, C. W. Photocyclization of Stilbenes and Related Molecules. In *Organic Reactions*; John Wiley & Sons, Ltd, 2005; pp 1−456..
(61) Sudhakar, A.; Katz, T. J. Directive Effect of Bromine on Stilbene Photocyclizations. an Improved Synthesis of [7]Helicene. *Tetrahedron Lett.* **1986**, *27* (20), 2231−2234.
(62) Beletskaya, I. P.; Cheprakov, A. V. The Heck Reaction as a Sharpening Stone of Palladium Catalysis. *Chem. Rev.* **2000**, *100* (8), 3009−3066.
(63) Zou, L.; Wang, X.-Y.; Shi, K.; Wang, J.-Y.; Pei, J. Fusion at the Non-K-Region of Pyrene: An Alternative Strategy To Extend the π-Conjugated Plane of Pyrene. *Org. Lett.* **2013**, *15* (17), 4378−4381.
(64) Zych, D.; Kubis, M. Bromopyrene Symphony: Synthesis and Characterisation of Isomeric Derivatives at Non-K Region and Nodal Positions for Diverse Functionalisation Strategies. *Molecules* **2024**, *29* (5), 1131.
(65) Yamato, T. Medium-Sized Cyclophanes. Part 31. Synthesis and Electrophilic Substitution of 8-Substituted [2]Metacyclo[2](1,3)-Pyrenophanes. *J. Chem. Soc., Perkin Trans. 1* **1993**, *11*, 3127−3137.
(66) Grimshaw, J.; Trocha-Grimshaw, J. Characterisation of 1.6- and I.8-Dibromopyrenes. *J. Chem. Soc., Perkin Trans. 1* **1972**, 1622−1623.
(67) Weber, J.; Clennan, E. L. Origin of the Preferential Formation of Helicenes in Mallory Photocyclizations. Temperature as a Tool to Influence Reaction Regiochemistry. *J. Org. Chem.* **2019**, *84* (2), 817−830.
(68) Hulley, E. B.; Clennan, E. L. Dihydrophenanthrene Open-Shell Singlet Diradicals and Their Roles in the Mallory Photocyclization Reaction. *J. Am. Chem. Soc.* **2024**, *146* (1), 1122−1131.
(69) Reyes, M. B.; Lobkovsky, E. B.; Carpenter, B. K. Interplay of Orbital Symmetry and Nonstatistical Dynamics in the Thermal Rearrangements of Bicyclo[n.1.0]Polyenes. *J. Am. Chem. Soc.* **2002**, *124* (4), 641−651.
(70) Hong, Y. J.; Tantillo, D. J. Branching Out from the Bisabolyl Cation. Unifying Mechanistic Pathways to Barbatene, Bazzanene, Chamigrene, Chamipinene, Cumacrene, Cuprenene, Dunniene, Isobazzanene, Iso-γ-Bisabolene, Isochamigrene, Laurene, Microbiotene, Sesquithujene, Sesquisabinene, Thujopsene, Trichodiene, and Widdradiene Sesquiterpenes. *J. Am. Chem. Soc.* **2014**, *136* (6), 2450−2463.
(71) Bailey, J. O.; Singleton, D. A. Failure and Redemption of Statistical and Nonstatistical Rate Theories in the Hydroboration of Alkenes. *J. Am. Chem. Soc.* **2017**, *139* (44), 15710−15723.
(72) Oruganti, B.; Pál Kalapos, P.; Bhargav, V.; London, G.; Durbeej, B. Photoinduced Changes in Aromaticity Facilitate Electrocyclization of Dithienylbenzene Switches. *J. Am. Chem. Soc.* **2020**, *142* (32), 13941−13953.
(73) Whitesell, J. K.; Minton, M. A.; Tran, V. D. The Non-Equilibration of Excited Rotamers (NEER) Principle. Ground-State Conformational Bias in Triene Photocyclizations. *J. Am. Chem. Soc.* **1989**, *111* (4), 1473−1476.
(74) Baird, N. C. Quantum Organic Photochemistry. II. Resonance and Aromaticity in the Lowest 3.Pi.Pi.* State of Cyclic Hydrocarbons. *J. Am. Chem. Soc.* **1972**, *94* (14), 4941−4948.
(75) Rosenberg, M.; Dahlstrand, C.; Kilså, K.; Ottosson, H. Excited State Aromaticity and Antiaromaticity: Opportunities for Photophysical and Photochemical Rationalizations. *Chem. Rev.* **2014**, *114* (10), 5379−5425.
(76) Karas, L. J.; Wu, J. I. Baird's Rules at the Tipping Point. *Nat. Chem.* **2022**, *14* (7), 723−725.
(77) Chen, Z.; Wannere, C. S.; Corminboeuf, C.; Puchta, R.; Schleyer, P. v. R. Nucleus-Independent Chemical Shifts (NICS) as an Aromaticity Criterion. *Chem. Rev.* **2005**, *105* (10), 3842−3888.
(78) Alabugin, I. V.; Manoharan, M.; Breiner, B.; Lewis, F. D. Control of Kinetics and Thermodynamics of [1,5]-Shifts by Aromaticity: A View through the Prism of Marcus Theory. *J. Am. Chem. Soc.* **2003**, *125* (31), 9329−9342.
(79) Lewis, F. D.; Sajimon, M. C.; Zuo, X.; Rubin, M.; Gevorgyan, V. Competitive 1,2- and 1,5-Hydrogen Shifts Following 2-Vinylbiphenyl Photocyclization. *J. Org. Chem.* **2005**, *70* (25), 10447−10452.
(80) Yang, W.; Monteiro, J. H. S. K.; de Bettencourt-Dias, A.; Catalano, V. J.; Chalifoux, W. A. Pyrenes, Peropyrenes, and Teropyrenes: Synthesis, Structures, and Photophysical Properties. *Angew. Chem., Int. Ed.* **2016**, *55* (35), 10427−10430.
(81) Kreyenschmidt, M.; Baumgarten, M.; Tyutyulkov, N.; Müllen, K. 2,2′-Bipyrenyl and Para-Terpyrenyl—A New Type of Electronically Decoupled Oligoarylene. *Angew. Chem., Int. Ed. Engl.* **1994**, *33* (19), 1957−1959.
(82) Bains, G. K.; Kim, S. H.; Sorin, E. J.; Narayanaswami, V. The Extent of Pyrene Excimer Fluorescence Emission Is a Reflector of Distance and Flexibility: Analysis of the Segment Linking the LDL Receptor-Binding and Tetramerization Domains of Apolipoprotein E3. *Biochemistry* **2012**, *51* (31), 6207−6219.
(83) Förster, Th.; Kasper, K. Ein Konzentrationsumschlag der Fluoreszenz des Pyrens. *Z. Elektrochem. Berichte Bunsenges. phys. Chem* **1955**, *59* (10), 976−980.
(84) Birks, J. B.; Christophorou, L. G. Excimer Fluorescence Spectra of Pyrene Derivatives. *Spectrochim. Acta* **1963**, *19* (2), 401−410.
(85) Birks, J. B.; Dyson, D. J.; Munro, I. H.; Flowers, B. H. Excimer' Fluorescence II. Lifetime Studies of Pyrene Solutions. *Proc. R. Soc. London, Ser. A* **1963**, *275* (1363), 575−588.
(86) McRae, E. G.; Kasha, M. Enhancement of Phosphorescence Ability upon Aggregation of Dye Molecules. *J. Chem. Phys.* **1958**, *28* (4), 721−722.
(87) Mallory, F. B.; Mallory, C. W. Photocyclization of Stilbenes and Related Molecules. In *Organic Reactions*; John Wiley & Sons, Inc: Hoboken, NJ, USA, 1984; pp 1−456..
(88) Lvov, A. G. Switching the Mallory Reaction to Synthesis of Naphthalenes, Benzannulated Heterocycles, and Their Derivatives. *J. Org. Chem.* **2020**, *85* (14), 8749−8759.
(89) Brink, M.; Möllerstedt, H.; Ottosson, C.-H. Characteristics of the Electronic Structures of Diabatically and Adiabatically Z/E-Isomerizing Olefins in the T1 State. *J. Phys. Chem. A* **2001**, *105* (16), 4071−4083.
(90) Kato, H.; Brink, M.; Möllerstedt, H.; Piqueras, M. C.; Crespo, R.; Ottosson, H. Z/E-Photoisomerizations of Olefins with 4npi- or (4n + 2)Pi-Electron Substituents: Zigzag Variations in Olefin Properties along the T(1) State Energy Surfaces. *J. Org. Chem.* **2005**, *70* (23), 9495−9504.
(91) Zeidan, T. A.; Kovalenko, S. V.; Manoharan, M.; Clark, R. J.; Ghiviriga, I.; Alabugin, I. V. Triplet Acetylenes as Synthetic Equivalents of 1,2-Bicarbenes: Phantom n,Π* State Controls Reactivity in Triplet Photocycloaddition. *J. Am. Chem. Soc.* **2005**, *127* (12), 4270−4285.
(92) Villaume, S.; Ottosson, H. Aromaticity Changes along the Lowest-Triplet-State Path for C = C Bond Rotation of Annulenyl-Substituted Olefins Probed by the Electron Localization Function. *J. Phys. Chem. A* **2009**, *113* (44), 12304−12310.

https://doi.org/10.1021/jacs.4c14486
J. Am. Chem. Soc. 2025, 147, 1074−1091

(93) Mohamed, R. K.; Mondal, S.; Gold, B.; Evoniuk, C. J.; Banerjee, T.; Hanson, K.; Alabugin, I. V. Alkenes as Alkyne Equivalents in Radical Cascades Terminated by Fragmentations: Overcoming Stereoelectronic Restrictions on Ring Expansions for the Preparation of Expanded Polyaromatics. *J. Am. Chem. Soc.* **2015**, *137* (19), 6335−6349.
(94) Zhu, J.; Fogarty, H. A.; Möllerstedt, H.; Brink, M.; Ottosson, H. Aromaticity Effects on the Profiles of the Lowest Triplet-State Potential-Energy Surfaces for Rotation about the C. *Chem. - Eur. J.* **2013**, *19* (32), 10698−10707.
(95) Singh, K.; Fennell, C. J.; Coutsias, E. A.; Latifi, R.; Hartson, S.; Weaver, J. D. Light Harvesting for Rapid and Selective Reactions: Click Chemistry with Strain-Loadable Alkenes. *Chem.* **2018**, *4* (1), 124−137.
(96) Saltiel, J.; Tarkalanov, N.; Sears, D. F. Conformer-Specific Adiabatic Cis .fwdarw. Trans Photoisomerization of cis-1-(2-Naphthyl)-2-phenylethene. A Striking Application of the NEER Principle. *Am. Chem. Soc.* **1995**, *117*, 5586−5587.
(97) Havinga, E.; Schlatmann, J. L. M. A. Remarks on the Specificities of the Photochemical and Thermal Transformations in the Vitamin D Field. *Tetrahedron* **1961**, *16* (1), 146−152.
(98) Hu, C.; Kuhn, L.; Makurvet, F. D.; Knorr, E. S.; Lin, X.; Kawade, R. K.; Mentink-Vigier, F.; Hanson, K.; Alabugin, I. V. Tethering Three Radical Cascades for Controlled Termination of Radical Alkyne Peri-Annulations: Making Phenalenyl Ketones without Oxidants. *J. Am. Chem. Soc.* **2024**, *146* (6), 4187−4211.
(99) Wu, X.; Zhu, C. Recent Advances in Ring-Opening Functionalization of Cycloalkanols by C−C σ-Bond Cleavage. *Chem. Rec.* **2018**, *18* (6), 587−598.
(100) Abe, M.; Inakazu, T.; Munakata, J.; Nojima, M. 18O-Tracer Studies of Fe(II)-Induced Decomposition of 1,2,4-Trioxolanes (Ozonides) Derived from Cyclopentenes and Indenes. Inner-Sphere Electron Transfer Reduction of the Peroxide Linkage. *J. Am. Chem. Soc.* **1999**, *121* (28), 6556−6562.
(101) Sakai, H. A.; MacMillan, D. W. C. Nontraditional Fragment Couplings of Alcohols and Carboxylic Acids: C(Sp3)−C(Sp3) Cross-Coupling via Radical Sorting. *J. Am. Chem. Soc.* **2022**, *144* (14), 6185−6192.
(102) Harris, T.; Gomes, G.; Clark, R. J.; Alabugin, I. V. Domino Fragmentations in Traceless Directing Groups of Radical Cascades: Evidence for the Formation of Alkoxy Radicals via C−O Scission. *J. Org. Chem.* **2016**, *81* (14), 6007−6017.
(103) Baroudi, A.; Mauldin, J.; Alabugin, I. V. Conformationally Gated Fragmentations and Rearrangements Promoted by Interception of the Bergman Cyclization through Intramolecular H-Abstraction: A Possible Mechanism of Auto-Resistance to Natural Enediyne Antibiotics? *J. Am. Chem. Soc.* **2010**, *132* (3), 967−979.
(104) Campbell, A.; Dos Santos, N. R.; Alabugin, I. Photochemical Uncaging of Aldehydes and Ketones via Photocyclization/Fragmentation Cascades of Enyne Alcohols: An Unusual Application for a Cycloaromatization Process. *Molecules* **2023**, *28* (15), 5704.
(105) Mondal, S.; Gold, B.; Mohamed, R. K.; Alabugin, I. V. Design of Leaving Groups in Radical C−C Fragmentations: Through-Bond 2c−3e Interactions in Self-Terminating Radical Cascades. *Chem. - Eur. J.* **2014**, *20* (28), 8664−8669.
(106) Baroudi, A.; Alicea, J.; Flack, P.; Kirincich, J.; Alabugin, I. V. Radical O→C Transposition: A Metal-Free Process for Conversion of Phenols into Benzoates and Benzamides. *J. Org. Chem.* **2011**, *76* (6), 1521−1537.

https://doi.org/10.1021/jacs.4c14486
J. Am. Chem. Soc. 2025, 147, 1074−1091